1   **Biophysical and proteomic analyses suggest functions of *Pseudomonas syringae* pv *tomato***

2   **DC3000 extracellular vesicles in bacterial growth during plant infection**

3

4   Martin Janda[1,2,+], Christina Ludwig[3], Katarzyna Rybak[1], Chen Meng[3], Egidio Stigliano[4,5], Leon

5   Botzenhardt[1], Beata Szulc[1], Jan Sklenar[4], Frank L.H. Menke[4], Jacob G. Malone[5,6], Andreas

6   Brachmann[1], Andreas Klingl[1] and Silke Robatzek[1#]

7

8   [1]LMU Biocenter, Ludwig-Maximilian-University of Munich, Großhaderner Strasse 4, 82152

9   Martinsried, DE

10   [2]University of Chemistry and Technology Prague, Department of Biochemistry and

11   Microbiology, Technická 5, Prague 6 – Dejvice 166 28, CZ

12   [3]Bavarian Center for Biomolecular Mass Spectrometry (BayBioMS), Technical University of

13   Munich, Gregor-Mendel-Strasse 4, 85354 Freising, DE

14   [4]The Sainsbury Laboratory, Norwich Research Park, NR4 7UH, UK

15   [5]John Innes Centre, Norwich Research Park, NR4 7UH, UK

16   [6]University of East Anglia, Norwich Research Park, NR4 7TJ, UK

17   [+]Present address: Faculty of Science, University of South Bohemia in České Budějovice,

18   Branišovská 1645/31a, České Budějovice, CZ

19

20   [#]Correspondence: Silke Robatzek

21   LMU Biocenter

22   Tel.: +49-2180-74124

23   Email: robatzek@bio.lmu.de

24

25

1

26   Short title: Analysis of *Pto* DC3000 extracellular vesicles

27

28   Key words: Extracellular vesicles, EVs, *Pto* DC3000, proteomics, pattern-triggered immunity,

29   PTI, nanoparticle tracking analysis, NTA, *Arabidopsis thaliana*

30

31   Manuscript information: Summary (180 words), text excluding references (10.450 words). The

32   number of figures: 8 main figures; 6 supplemental figures; 2 main tables; 6 supplemental tables.

Summary

Vesiculation is a process employed by Gram-negative bacteria to release extracellular vesicles (EVs) into the environment. Bacterial EVs contain molecular cargo from the donor bacterium and play important roles in bacterial survival and growth. Here, we describe EV production in plant-pathogenic *Pseudomonas syringae* pv. *tomato* DC3000 (*Pto* DC3000), the causal agent of bacterial speck disease. Cultured *Pto* DC3000 exhibited EV structures both on the cell surface and in the vicinity of bacterial cells, observed as outer membrane vesicle (OMV) release. We used in-solution trypsin digestion coupled to mass spectrometry to identify 369 proteins enriched in EVs recovered from cultured *Pto* DC3000. The predicted localization profile of EV proteins supports the production of EVs also in the form of outer-inner-membrane vesicles (OIMVs). EV production varied slightly between bacterial lifestyles and also occurred *in planta*. The potential contribution of EVs to *Pto* DC3000 plant infection was assessed using plant treatments and bioinformatic analysis of the EV-enriched proteins. While these results identify immunogenic activities of the EVs, they also point at roles for EVs in bacterial defences and nutrient acquisition by *Pto* DC3000.

Introduction

Successful colonization of hosts depends on the ability of microbes to defend themselves against host immune responses and acquire nutrients. Bacterial pathogens use macromolecular translocation systems and deliver virulence proteins, so-called effectors, to circumvent host immunity (Buttner & Bonas, 2010). *Pseudomonas syringae* pv. *tomato* (*Pto*) DC3000 is the causal agent of bacterial speck, a common disease that occurs in tomato production worldwide (Mansfield *et al.*, 2012, Wilson *et al.*, 2002). *Pto* DC3000 is a Gram-negative bacterium that invades through openings in the plant surface and propagates in the apoplast, where it takes up nutrients and proliferates (Melotto *et al.*, 2006, Xin & He, 2013, Xin *et al.*, 2018). Plants

58 respond rapidly to colonization by microbes, activating innate defence strategies, which can

59 broadly be categorized into pattern-triggered immunity (PTI) activated by microbe-associated

60 molecular patterns (MAMPs) and effector-triggered immunity (ETI) induced upon recognition

61 of virulence factors or their actions (Couto D. & Zipfel, 2016, Dodds & Rathjen, 2010).

62 Virulence of *Pto* DC3000 largely depends on the Type-III secretion system and its secreted

63 effectors (Kvitko *et al.*, 2009, Nobori *et al.*, 2018, Nobori *et al.*, 2019, Nomura *et al.*, 2006). A

64 number of Type-III secreted effectors from *Pto* DC3000 and their *in planta* targets have been

65 identified, many involved in immune suppression and some with roles in gaining access to

66 nutrients (Wei *et al.*, 2018, Xin *et al.*, 2018). For example, genes encoding proteins for

67 siderophore biosynthesis are upregulated *in planta* (Nobori *et al.*, 2018). In addition, pathogenic

68 bacteria need to adapt to the host environment, resisting the defences induced by the host

69 immune system.

70

71 The survival of infectious Gram-negative bacteria is greatly enhanced by releasing extracellular

72 vesicles (EVs), a process widely studied in the context of bacteria pathogenic to humans

73 (Schwechheimer & Kuehn, 2015). During infection, bacterial EVs can counteract the effect of

74 antimicrobial peptides (Roszkowiak *et al.*, 2019). They also perform immunomodulatory

75 functions by delivering virulence factors to recipient cells resulting in immune-suppression

76 (Kaparakis-Liaskos & Ferrero, 2015), despite having the capacity to activate defences due to

77 their immunogenic cargoes (Kaparakis-Liaskos & Ferrero, 2015). More recently, a number of

78 studies provide evidence that plant pathogenic bacteria, including cultured *Pto* bacteria release

79 EVs (Bahar *et al.*, 2016, Chowdhury & Jagannadham, 2013, McMillan *et al.*, 2020). Although

80 insights into both immunogenic and virulent roles have been achieved, little is currently known

81 about the importance of EV production in bacterial infection success.

82

83   EVs are cytosol-containing membrane "nano" spheres that provide selection, storage and

84   protection against degradation of enclosed cargoes in a highly dynamic and environmental cue-

85   responsive manner (Bielska *et al.*, 2019, Rybak & Robatzek, 2019, Schwechheimer & Kuehn,

86   2015). Gram-negative bacteria actively form EVs by budding and shedding of the outer

87   membrane, producing so-called outer membrane vesicles (OMVs) (Raposo & Stoorvogel,

88   2013, Roier *et al.*, 2016). Outer-inner-membrane vesicles (OIMVs) have also been described,

89   involving a different mode of release such as endolysin-triggered cell lysis (Perez-Cruz *et al.*,

90   2015, Toyofuku *et al.*, 2019). EVs can also be produced in the form of elongated, tube-shaped

91   vesicles as observed in Gram-negative *Francisella* spp. (McCaig *et al.*, 2013, Sampath *et al.*,

92   2018). As insufficient biomarkers are available to convincingly probe their origin, in particular

93   for *P. syringae*, we will collectively refer to these vesicles as EVs. Notably, EV formation seems

94   to be an essential process since no bacterial mutant lacking vesicle release has been reported so

95   far and genetic reduction of vesiculation results in mutants with growth defects (McBroom *et*

96   *al.*, 2006).

97

98   Previous studies revealed a number of molecular cargoes present in EVs from phytopathogenic

99   bacteria of the *Agrobacterium tumefaciens*, *P. syringae*, *Xanthomonas campestris* and *Xylella*

100   *fastidiosa* species. These EV-associated proteins include degradative enzymes, Type-II-

101   secreted virulence-associated proteins, components of the Type-III secretion system and its

102   secreted proteins (Feitosa-Junior *et al.*, 2019, Chowdhury & Jagannadham, 2013, Knoke *et al.*,

103   2020, Nascimento *et al.*, 2016, Sidhu *et al.*, 2008, Sole *et al.*, 2015). While respective genetic

104   deletions of EV-associated degradative enzymes reduced bacterial virulence, the role of EVs in

105   their delivery remained unanswered (Nascimento *et al.*, 2016, Sidhu *et al.*, 2008, Sole *et al.*,

106   2015). A previous seminal study described the production of EVs as a mechanism, by which *X.*

107   *fastidiosa* regulates its attachment to host cells and thus the promotes systemic infection

108 (Ionescu *et al.*, 2014). However, elongation factor Tu (EF-Tu) and lipopolysaccharides (LPS)

109 are abundant components of EVs from *P. syringae*, *X. campestris*, *X. oryzae* and *X. fastidiosa*

110 (Bahar *et al.*, 2016, Feitosa-Junior *et al.*, 2019, Chowdhury & Jagannadham, 2013, Sidhu *et al.*,

111 2008). Both represent MAMPs, with EV-associated EF-Tu shown to activate a prototypic PTI

112 response in a receptor-dependent manner (Bahar *et al.*, 2016). Further results indicate that EV-

113 induced immunity, triggered with EVs recovered from pathogenic *Pto* DC3000 and the

114 commensal *P. fluorescens*, protects plants against *Pto* DC3000 infection (McMillan *et al.*,

115 2020). These studies hint at some contrasting roles that EVs from bacterial phytopathogens

116 could play during plant infection.

117

118 Here, we used nanoparticle tracking analysis (NTA) to describe the production and the

119 biophysical properties of EVs from *Pto* DC3000 in different growth conditions including their

120 accumulation *in planta*. Analysis of *Pto* DC3000 cellular, outer membrane (OM) and EV

121 proteomes by mass spectrometry identified 369 EV-enriched proteins. The potential

122 contribution to bacterial growth *in planta* of these proteins was assessed using bioinformatic

123 analysis as well as exploring plant responses to EVs. These findings expand our understanding

124 of the functions of EVs in bacterial infection of plants.

125

126 **Results**

127 ***Pto* DC3000 bacteria vesiculate and produce EVs in culture**

128 We first examined the morphology of *Pto* DC3000 cultures by scanning electron microscopy

129 (SEM). The bacteria displayed multiple spherical structures protruding from their cell surfaces,

130 with diameters in the range of 20-120 nm (Fig. 1A; S1A). These vesicle-like structures appeared

131 to be released from the surface, as similarly sized vesicular structures could also be observed in

132 the vicinity of the bacteria (Fig. S1A). To determine whether these structures were released

6

133   from the bacterial cell surface, supernatants of planktonic *Pto* DC3000 cultures were filtered

134   through 0.22µm-pore membranes to remove intact bacteria and measured by Nanoparticle

135   Tracking Analysis (NTA) before (fluid sample) and after sucrose density gradient

136   centrifugation followed by ultracentrifugation (gradient-enriched sample) (Fig. S2A). Density

137   gradient centrifugation is used to separate EVs from other extracellular materials (Klimentova

138   & Stulik, 2015). NTA measures particle number (concentration), particle size (median diameter

139   and distribution), and particle surface charge (mean ζ-potential). Both sample types exhibited a

140   polydisperse sized population of spherical structures with a diameter ranging from ~ 50 to 200

141   nm and median sizes of 100 nm and 115 nm for fluid samples and gradient enriched samples,

142   respectively (Fig. 1C, 1G, S1B). This could suggest that *Pto* DC3000 releases vesicles from

143   different biogenesis routes.

144

145   Pellets obtained from gradient enriched samples were further examined by SEM and revealed

146   numerous spherical structures (Fig. 1B), yet in this analysis the vesicles diameter ranged

147   between 25 and 170 nm with a median around 50 nm. It is possible that conditions used for

148   SEM and NTA differ in their capacity to hydrate the vesicles and/or that NTA underestimates

149   smaller particles (Bachurski *et al.*, 2019). In addition, co-purifying filamentous structures could

150   be detected (Fig. 1B). To determine whether EV production is an active process, EVs were

151   quantified from culture supernatants of *Pto* DC3000 over cultivation time, with increasing

152   particle numbers observed with bacterial density (Fig. 1D, 1E, S2B). While the total amount of

153   EVs recovered from bacteria at late exponential growth was higher compared with early growth

154   stages (Fig. 1D, 1E), calculation of the amount of EVs produced per bacteria showed that

155   numbers were similar between growth stages (Fig. 1E). The median diameter and ζ-potential of

156   EVs was comparable across growth stages (Fig. 1F, 1G, 1H).

157

158   Quantification of EVs from *Pto* DC3000 cultures that were incubated in fresh media followed

159   by heat inactivation showed increased vesicle numbers (Fig. 1D). This suggests that heat

160   inactivation could additionally trigger the production of vesicles, i.e. from cellular debris and/or

161   through a process described as explosive cell lysis (Toyofuku *et al.*, 2019). Given this increase

162   and the distinct size of the vesicles from heat inactivated bacterial cultures (Fig. 1F), it suggests

163   that the vesicles recovered from culture samples without heat inactivation are predominantly

164   produced from bacteria as an active process.

165

166   EVs were also isolated from biofilm grown *Pto* DC3000 cultures (Fig. S2C, S2D). The median

167   diameter of these EVs was smaller compared with EVs from planktonic gradient enriched *Pto*

168   DC3000 EVs but had a similar size to EVs from fluid samples (Fig. 1G). The mean ζ-potential

169   of EVs from biofilm samples was similar to EVs from planktonic gradient enriched samples

170   but more negative than EVs from fluid samples of planktonic *Pto* DC3000 cultures (Fig. 1H).

171   Thus, EVs show diverse biophysical properties depending on bacterial lifestyle, further refuting

172   the possibility that the purified particles are solely formed through nonspecific assembly of shed

173   membrane fragments.

174

8
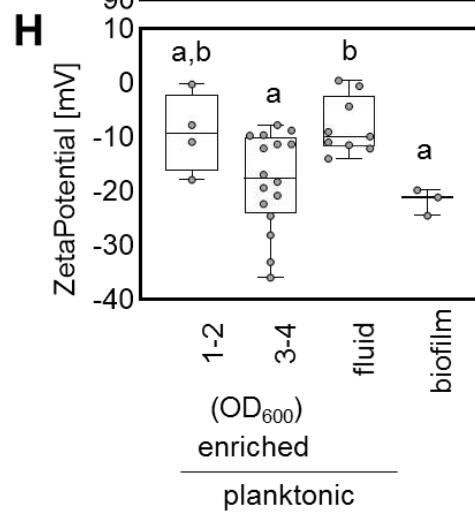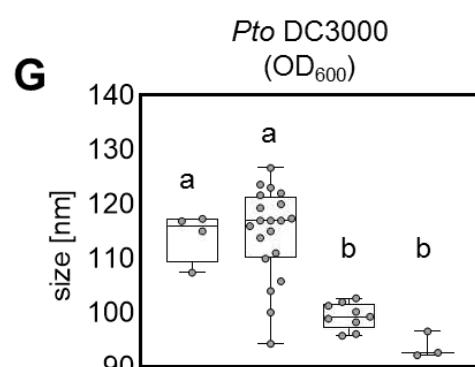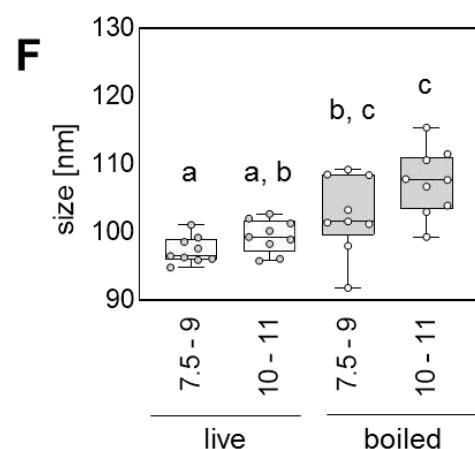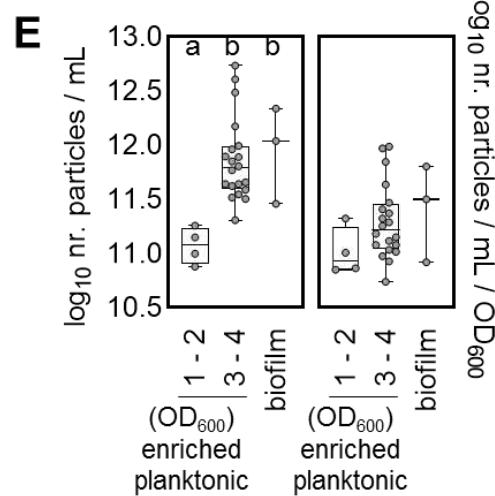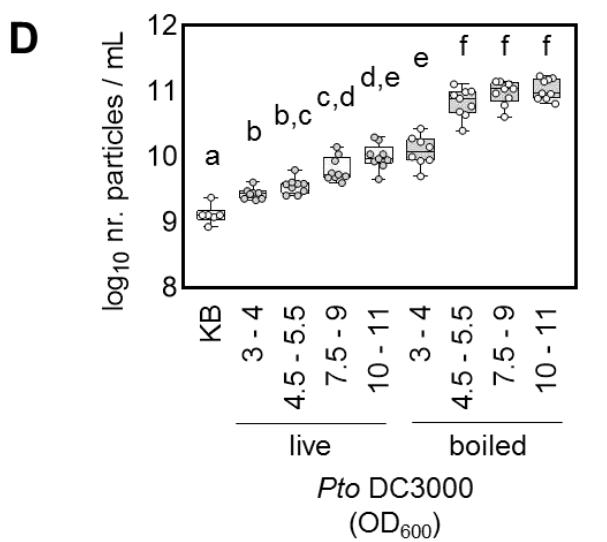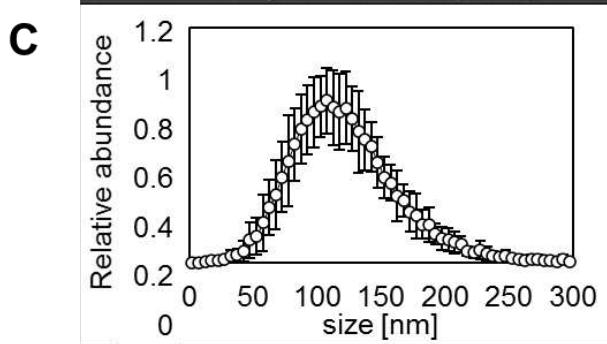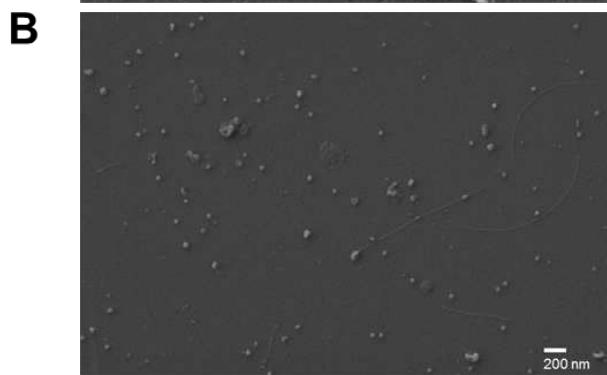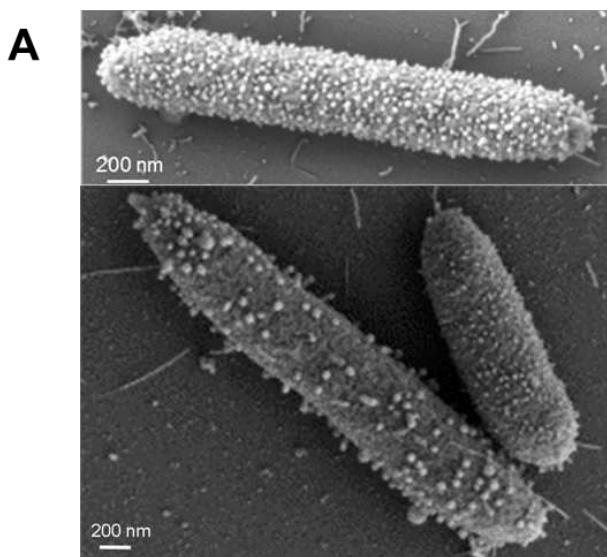
Figure 1. *Pto* DC3000 release extracellular vesicles with differing biophysical parameters depending on lifestyle. A) Representative SEM micrographs of *Pto* DC3000 growth in planktonic culture ($OD_{600} = 3-4$). **B)** Representative SEM micrograph of gradient enriched *Pto* DC3000 EVs purified from planktonic culture ($OD_{600} = 3-4$); scale bars represent 200 nm. For A and B, the micrographs were selected as representatives from three independent samples. For D-H each dot in the boxplot represents an independent sample. **C)** Size profile of gradient enriched EVs from *Pto* DC3000 planktonic cultures ($OD_{600} = 3-4$), the values represent mean and standard deviations from n = 20. Concentration **(D)** and size **(F)** of EVs from fluid samples before (live) and after heat inactivation of bacteria (boiled); King's B (KB) medium. Concentration **(E)**, size **(G)** and ζ-potential **(H)** of EVs from planktonic cultures (enriched = gradient enriched $OD_{600} = 1-2$ and 3-4 and fluid samples $OD_{600} = 7.5 - 11$) and of EVs from biofilm cultures. For D and F n = 8-9 independent samples, for samples in E and G n = 4 for $OD_{600} = 1-2$ and n = 20 for $OD_{600} = 3-4$ for gradient enriched samples, n = 9 for fluid samples and n=3 for biofilm. The box in boxplots extends from 25th to 75th percentiles, whiskers go down to the minimal value and up to the maximal value, the line in the middle of the box is plotted at the median. Different letters indicate significant (Welsch´s ANOVA with Dunnett´s T3 multiple comparisons post hoc test; $p < 0.05$).

175

176 To investigate whether the biophysical parameters of *Pto* DC3000 EVs could change upon

177 mechanical treatments, we subjected the samples to sonication, heating and freezing. In

178 addition, we tested the effect of incubation with Proteinase K, a treatment used to deplete the

179 EV samples of extravesicular proteins (Metruccio *et al.*, 2016). None of the treatments

180 significantly affected the particle concentration (Fig. 2). Also, particle size was not significantly

181 changed upon sonication and Proteinase K treatments (Fig. 2A, 2D). A significant increase in

182 particle size was observed after ten freeze-thaw cycles and longer heat exposure (Fig. 2B, 2C).

183 These observations suggest that EVs are affected by more extreme temperature treatments,

184 maybe forming higher aggregates, while sonication, shorter heat incubation, fewer freeze-thaw

185 cycles and Proteinase K treatments showed no significant effects.

186
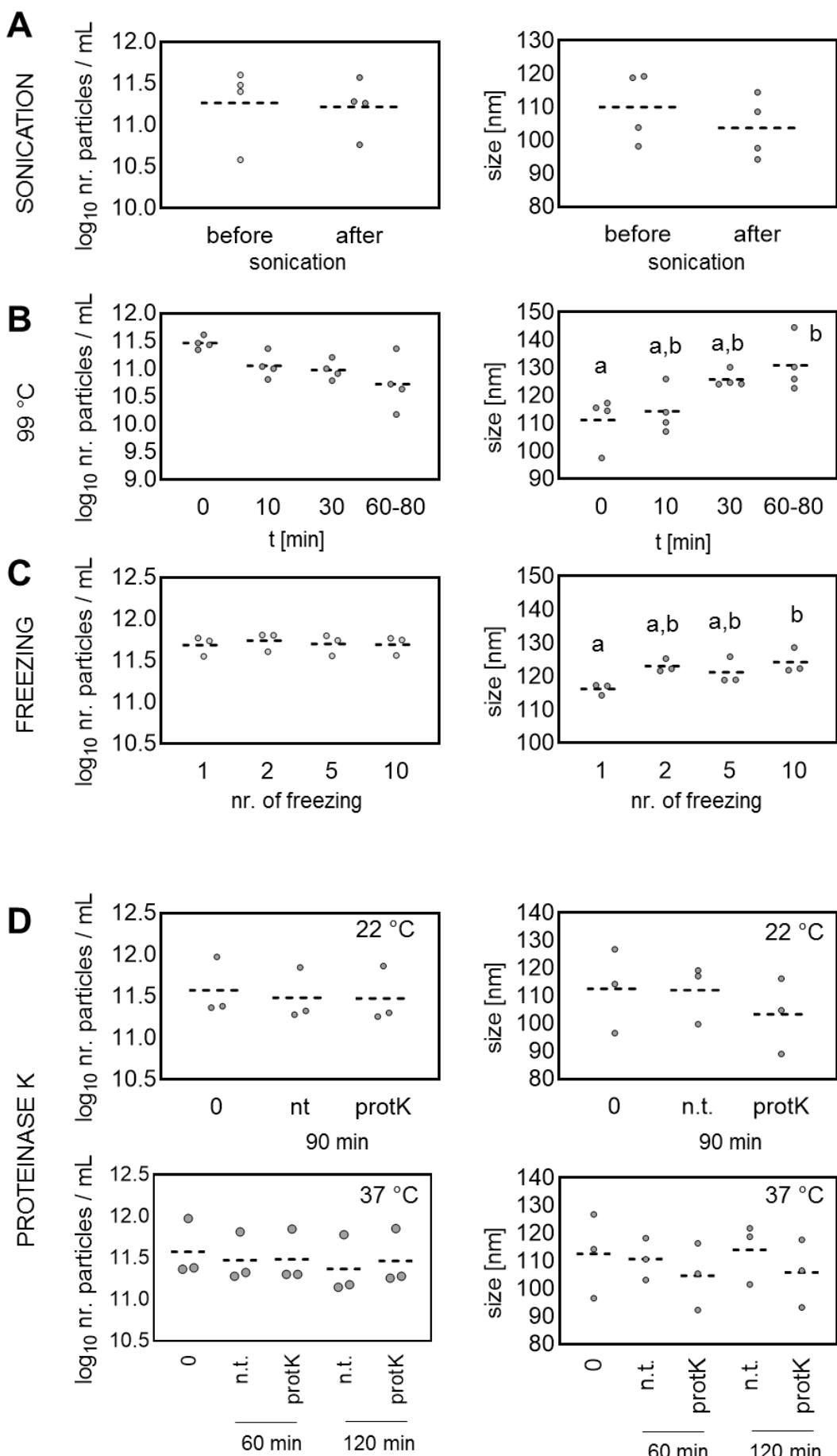
Figure 2. Disruptive treatments cause minor changes to biophysical parameters of gradient enriched EVs. Concentration and size analysis of *Pto* DC3000 EVs from planktonic cultures (OD_{600} = 3-4). Effects of **A)** sonication (10 times 30 s); **B)** 99 °C for 80 min; **C)** freezing and thawing (up to ten times); **D)** Proteinase K treatment (10 µg/mL) at 22 °C and 37 °C for up to 120 min. Individual circles represent particles characteristics from independent samples; n = 3 to 4. Different letters indicate significant difference (One-way ANOVA with Tukey post hoc test; $p < 0.05$).

187

188   ***Pto* DC3000 bacteria produce EVs *in planta***

189   To determine whether *Pto* DC3000 releases vesicles *in planta*, apoplastic fluids were recovered

190   from *Pto* DC3000-infected and control-treated *A. thaliana* leaf tissues at different time points.

191   The apoplastic fluids were collected, filtered to remove intact bacteria and then directly

192   characterized by NTA without density gradient centrifugation and ultracentrifugation. In these

193   apoplastic fluid samples, we identified particles with a median diameter of ~96 nm (Fig. 3A),

194   which increased in abundance upon infection with *Pto* DC3000 (Fig. 3B), consistent with

195   previous findings (Rutter & Innes, 2017). Increased particle abundance correlated with the

196   bacterial infection time and titers (Fig. 3B, Fig. S3A, S3B). We also analysed EVs from

197   apoplastic fluids of plants, which were co-treated with 100 nM flg22 and *Pto* DC3000. Particle

198   numbers were lower than those recovered from *Pto* DC3000 infection only, consistent with

199   induced plant defences (Fig. S3C). Taken together, the higher particle numbers and

200   polydisperse particle size isolated from *Pto* DC3000-infected plants compared to flg22

201   immune-stimulated plants hints at bacterial-derived EVs present in *A. thaliana* apoplastic fluids

202   (Fig. 3B).

203

204   Since *Pto* DC3000 (fluid sample) and *A. thaliana* (apoplastic fluid samples) EVs did not

205   significantly differ in diameter (Fig. 1G, 3A), we focused on the charge of EVs, reflecting the

206   different surface composition of bacterial (prokaryotic) and plant-derived (eukaryotic) EVs.

207   Evaluation of the mean ζ-potential identified significantly less negatively charged EVs

208   recovered from apoplastic fluids of *Pto* DC3000-infected plants at three days post infection

209   compared with control treatments and earlier time points (Fig. 3C, 3D, 3E, 3G). This time point

210   correlated with *in planta* bacterial proliferation and depended on bacterial inoculum (Fig. S3A,

211   S3B). Plotting the relative particle abundance over particle charge, the ζ-potential profiles of

212   EVs recovered from apoplastic fluids of untreated, control-treated and flg22-treated *A. thaliana*

213   identified major peaks around -32 mV (Fig. 3C, 3D, S3J). By contrast, the ζ-potential profile of

214   EVs recovered from apoplastic fluids of *Pto* DC3000-infected *A. thaliana* had a broader

215   distribution with a similar major peak around -32 mV and an additional shoulder around -10

216   mV (Fig. 3E, 3G). Comparison of the different ζ-potential profiles revealed similarities of the

217   major -32 mV peak across all plant samples, likely representing a plant-derived EV pool (Fig.

218   3C, 3D, S3J, S3K). Notably, the shoulder around -10 mV detected from apoplastic fluids of *Pto*

219   DC3000-infected plant samples showed large overlay with the ζ-potential profile of EV

220   recovered from *Pto* DC3000 cultures (fluid samples), with a peak from -20 to 0 mV (Fig. 3E,

221   3F, 3G). This could, therefore, represent a bacterial-derived EV pool. Since the ζ-potential

222   profiles of EVs recovered from apoplastic fluids of flg22-treated *A. thaliana* did not differ

223   between untreated or control-treated leaves (Fig. 3C, S3J, S3K), we found no evidence that

224   plant EVs modulate their surface charge during infection. Thus, our data strongly suggest that

225   *Pto* DC3000 release EVs during plant infection.

226

13
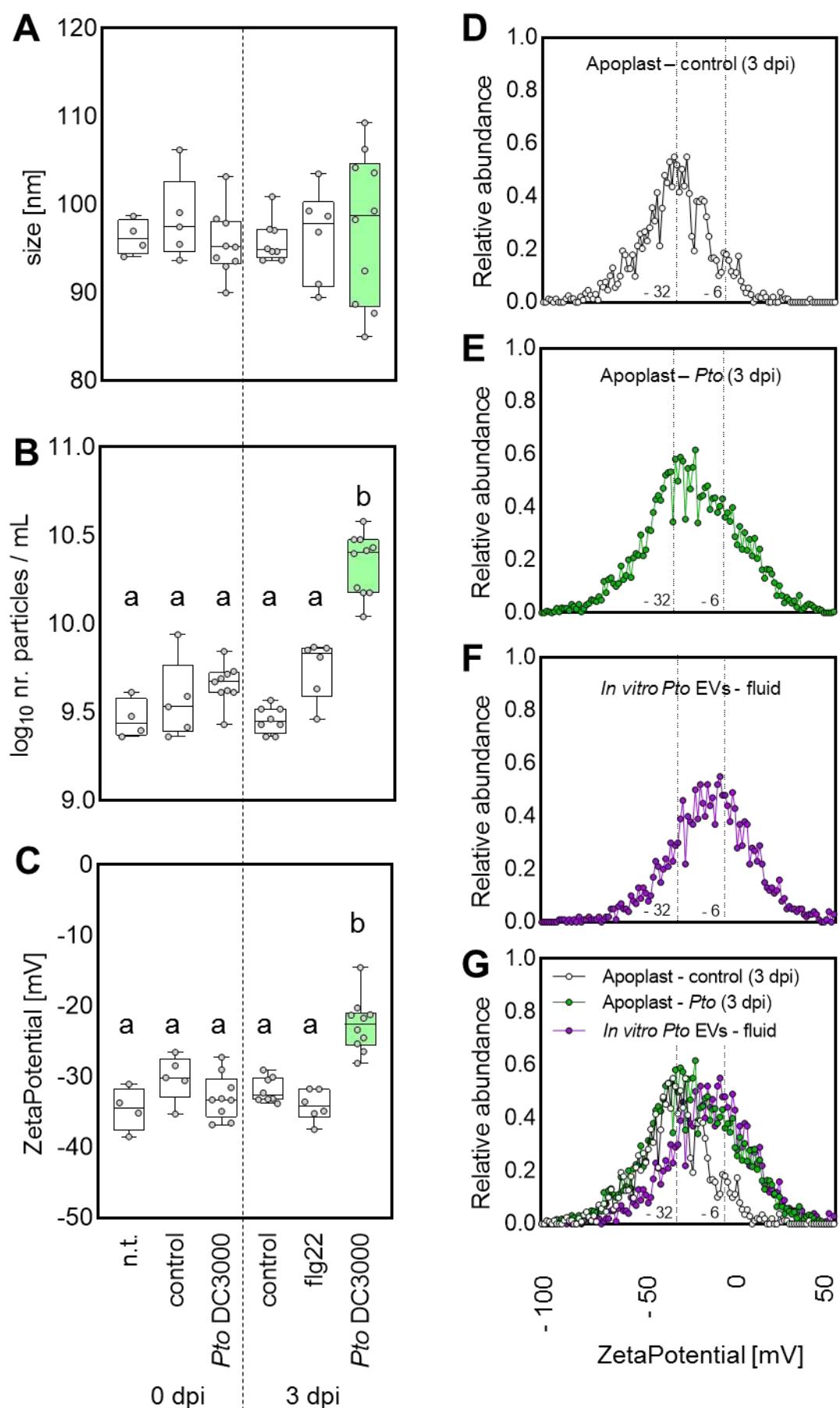
Figure 3. *Pto* DC3000 release EVs *in planta*. Size, concentration and charge measurements of apoplastic fluids from *A. thaliana* plants infected with *Pto* DC3000 and treated as indicated. **A)** Size of the particles. **B)** Particle concentration in apoplastic fluids. **C)** ζpotential of the particles. For A-C the variants represent: n.t. – non-treatment; control – 10 mM $MgCl_2$; *Pto* DC3000 (OD_{600} = 0.0006); 100 nM flg22. **D-G)** The profile of ζ-potential for particles detected in Arabidopsis apoplast treated with $MgCl_2$ (control; D) for 3 days, with *Pto* DC3000 (*Pto*; OD_{600} = 0.0006; E) for 3 days and for EVs from *Pto* DC3000 grown in culture (fluid; F). The dots represent the mean from 8 (D, G_white), 10 (E, G_green) and 13 (F, G_purple). For A-C each dot in the boxplot represents an independent sample. The box in boxplots extends from 25th to 75th percentiles, whiskers go down to the minimal value and up to the maximal value, the line in the middle of the box is plotted at the median. Different letters indicate significant difference (One-way ANOVA with Tukey post hoc test; $p < 0.05$). The green colour is highlighting the particles from *Pto* DC3000 infected plants (3 dpi).

227

EV samples purified from *Pto* DC3000 cultures trigger plant immune responses

228

229 Bacterial EVs contain immunogenic molecules such as EF-Tu and LPS, and can contain

230 digestive enzymes and effectors that undermine host defences (Bahar *et al.*, 2016, Feitosa-

231 Junior *et al.*, 2019, Knoke *et al.*, 2020, Rybak & Robatzek, 2019). To determine the effect of

232 EVs from *Pto* DC3000 on plant cells, we first examined the ability of the *Pto* DC3000 EVs to

233 modulate the outcome of bacterial infection. We pre-treated *A. thaliana* leaves with *Pto*

234 DC3000 EVs, which limited the growth of subsequently infected *Pto* DC3000 bacteria *in planta*

235 (Fig. 4A, S4A). Thus, the immunogenic potential of *Pto* DC3000 EVs is sufficient to restrict

236 bacterial colonization, consistent with recent observations (McMillan *et al.*, 2020). Since

237 MAMP treatment mediates anti-bacterial protection through the induction of plant immune

238 reactions (Zipfel *et al.*, 2004), we next evaluated defence gene expression to EV treatment using

239 *pFRK1*::GUS reporter lines (Kunze *et al.*, 2004). Seedlings were treated with purified EVs

240 isolated from *Pto* DC3000 cultures, and GUS staining was measured after 18 h. We observed a

241 significant induction of *pFRK1*::GUS expression triggered by the EVs albeit lower when

242 compared to flg22 treatments (Fig. 4B, 4C). EV-induced *FRK1* upregulation is in agreement

243 with previous observations (Bahar *et al.*, 2016). We also tested whether treatment with *Pto*

244 DC3000 EVs could arrest seedling growth, a prototypic PTI response of plants to continual

245 MAMP stimulation (Bredow *et al.*, 2019). Unexpectedly, we observed no significant growth

15

246   reduction (Fig. 4D). This suggests that immune induction by *Pto* DC3000 EVs does not affect

247   plant growth, unlike treatment with flg22 (Fig. S4B) (Bredow *et al.*, 2019).

248

249   A previous study demonstrated that bacterial (*X. campestris*) EV activation of *FRK1* expression

250   depends on the EF-Tu Receptor (EFR), which is responsible for detection of the immunogenic

251   peptide elf18 derived from bacterial EF-Tu (Bahar *et al.*, 2016, Zipfel *et al.*, 2006). To

252   determine the pathway, by which the *Pto* DC3000 EVs trigger immune responses, we treated

253   *efr-1* and *flagellin sensing 2* (*fls2*) mutants, the latter responsible for recognition of the

254   immunogenic peptide flg22 of bacterial flagellin in *A. thaliana* (Zipfel *et al.*, 2004), with *Pto*

255   DC3000 EVs and monitored *FRK1* gene expression. The *Pto* DC3000 EVs triggered *FRK1*

256   gene expression in wild type and *efr-1* mutants to similar levels (Fig. 4E). No *FRK1* induction

257   was observed in *fls2* mutants. Thus, the EVs isolated from *Pto* DC3000 cultures must contain

258   bacterial flagellin. Notably, SEM analysis of gradient enriched EV samples showed the co-

259   purification of filament-like structures (Fig. 1B), which could represent detached bacterial

260   flagellar or pili. This suggests that co-purifying flagellin molecules may trigger plant immune

261   responses.

262

16
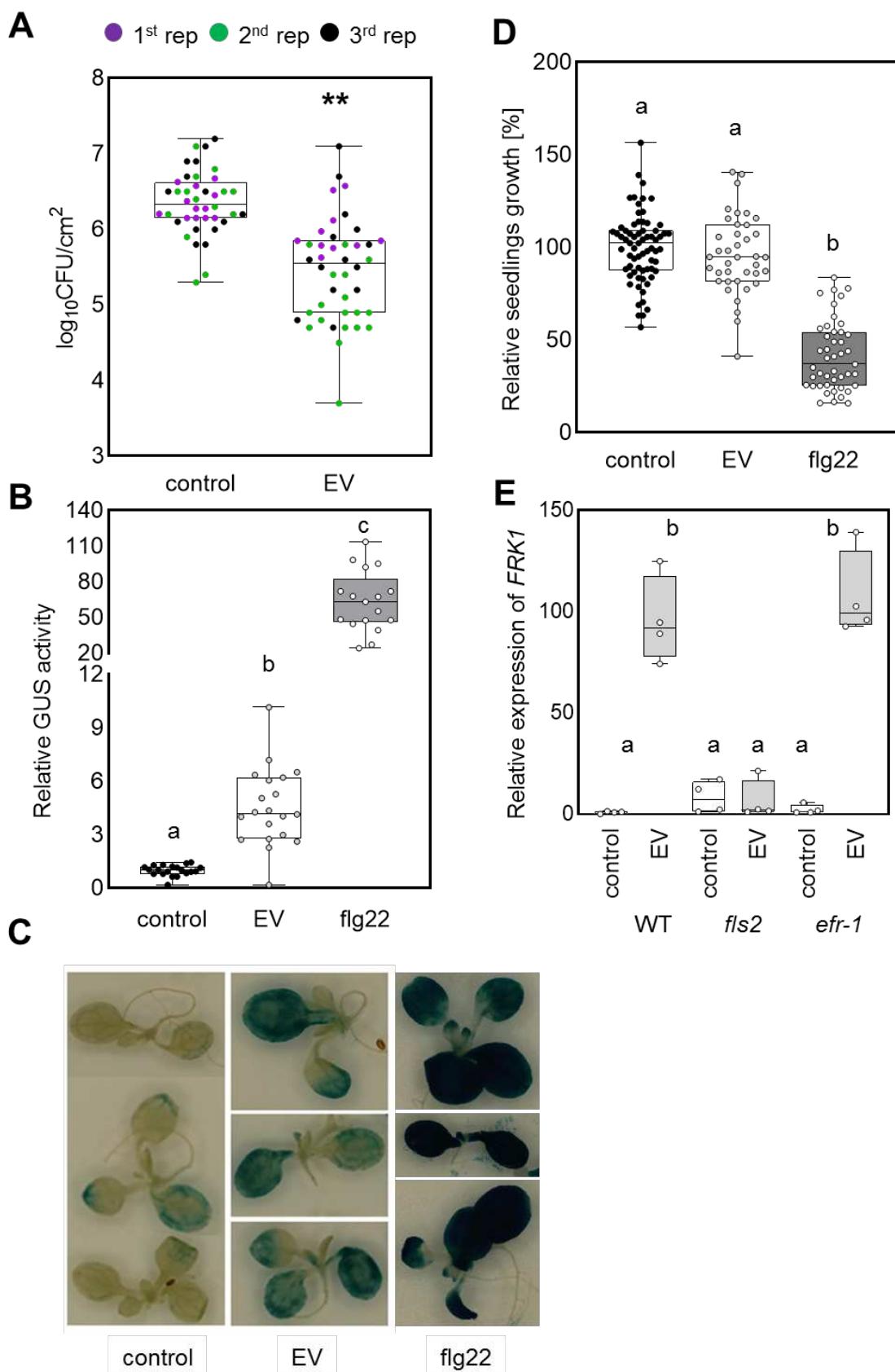
Figure 4. Immunogenic effects of *Pto* DC3000 EVs. A) *Pto* DC3000 growth (CFU) after infection into leaves of *A. thaliana* without and with EV pre-treatment at 3 dpi (control = 0.02 mM EDTA). Three biological repeats consisting each 12 independent samples were

performed. The dots with the same colour represent independent samples from one biological repeat. **B)** Quantification of *pFRK1*::GUS activity in seedlings incubated without and with EVs (concentration $\approx 1.10^{10}$) or with 100 nM flg22 for 18 h. **C)** Representative pictures of *pFRK1*::GUS seedlings incubated without and with EVs (concentration $\approx 1.10^{10}$) or with 100 nM flg22 for 18 h. **D)** Fresh weight of seedlings grown without and with EVs (concentration $\approx 1.10^{10}$) for 8 days. For control n = 69; for 100 nM flg22 treatment n = 44 and for EV treatment n = 39 of independent samples. **E)** Relative *FRK1* gene expression in seedlings of the indicated genotypes incubated without and with EVs (concentration $\approx 1.10^{10}$) for 5 h (control = 0.02 mM EDTA), four independent samples were used for each variant. For A, B, D, E each dot in the boxplot represents an independent sample. The box in boxplots extends from 25th to 75th percentiles, whiskers go down to the minimal value and up to the maximal value, the line in the middle of the box is plotted at the median. Asterisks indicate statistical significances (two tailed Welsch´s t-test; $p < 0.01$) in A; different letters indicate significant differences (Welsch´s ANOVA with Dunnett´s T3 multiple comparisons post hoc test; $p < 0.05$)) in B, D and E.

263

EVs from cultured *Pto* DC3000 are enriched in proteins with predicted roles in transport

and antimicrobial peptide resistance

To gain insights into the function of *Pto* DC3000 EVs during the infection process, we

characterized the proteome of EVs using liquid chromatography-based tandem mass

spectrometry (LC-MS/MS). The *Pto* DC3000 EV-associated proteins were isolated from

planktonic *Pto* DC3000 cultures by gradient enrichment. The proteomes of whole cells (WC)

(Park *et al.*, 2014) and the outer membrane (OM) (Choi *et al.*, 2011) from bacteria grown to

late exponential phase (OD_{600} = 3-4; Fig. S2B) were also analysed and compared with the EV

proteome. As expected, we detected the most proteins from the WC sample (n = 1587), followed

by the EV sample (n = 890) and 212 proteins in OM samples (Fig. 5A, Table S1). In total, 2898

proteins were identified over all samples, of which 1899 proteins were identified at least in three

samples per sample type (WC, EV or OM). These proteins were taken forward for further

analysis (Table S1). Similar protein intensity distributions were obtained for all samples (LFQ

values were generated by MaxQuant, Fig. S5) and the four replicate measurements per sample

type fell into sample clusters on the first and second principal components, suggesting a

systematic difference in the proteomes of these three sample types (Fig. 5B). By comparing the

proteomes of EV and WC, we identified 369 EV-enriched proteins, consisting of 162 proteins

18

281 exclusively identified in at least three replicates of EV sample (EV unique; Fig. 5C) and 207

282 proteins significantly higher in the EV compared with WC (Fig. 5C; Table S1).

283

284 Of the nine labelled highly-enriched EV and the five EV-unique proteins (Fig. 5C), eight have

285 unknown subcellular localization (PSPTO_3807; PSPTO_4822; PSPTO_0894; PSPTO_3407;

286 PSPTO_3424; PSPTO_3970, PSPTO_3396; and PSPTO_3409). This could indicate that these

287 proteins are predominantly present in EVs, a localization not included in the predictions. Four

288 proteins are annotated as lipoproteins, reported in other Gram-negative bacteria to mediate the

289 cross-linking of the peptidoglycan (PG) layer with the OM and thus playing roles in the

290 production of OMVs (Schwechheimer and Kuehn, 2015). PSPTO_3409 is the locus tag for the

291 ATP-dependent ClpP-1 protease. Clp proteases were previously shown to regulate quorum

292 sensing, in turn affecting OMV production and biofilm formation (Figaj *et al.*, 2019, Hall *et al.*,

293 2017). The other were annotated as hypothetical proteins.

294

295 The EV-enriched proteome included proteins related to virulence (Fig. 5C, Table S1), such as

296 MucD (PSPTO_4221) (Wang *et al.*, 2019), HopAJ2 (PSPTO_4817) (Vinatzer *et al.*, 2006) and

297 HopAH2-2 (PSPTO_3293) (Lovelace *et al.*, 2018, Schechter *et al.*, 2006). A major function of

298 virulence proteins is the suppression of PTI (Block & Alfano, 2011). To test whether *Pto*

299 DC3000 EVs could suppress a prototypic PTI response, we pre-treated leaves with EVs from

300 cultured bacteria 24 h before eliciting a ROS burst with MAMPs (flg22, elf18). EV pre-

301 treatments neither significantly reduced nor increased the MAMP-induced ROS production

302 (Fig. 6A). This suggests that under the tested conditions, *Pto* DC3000 EVs are not

303 predominantly involved in immune inhibition and/or further enhancing MAMP responses.

304

19
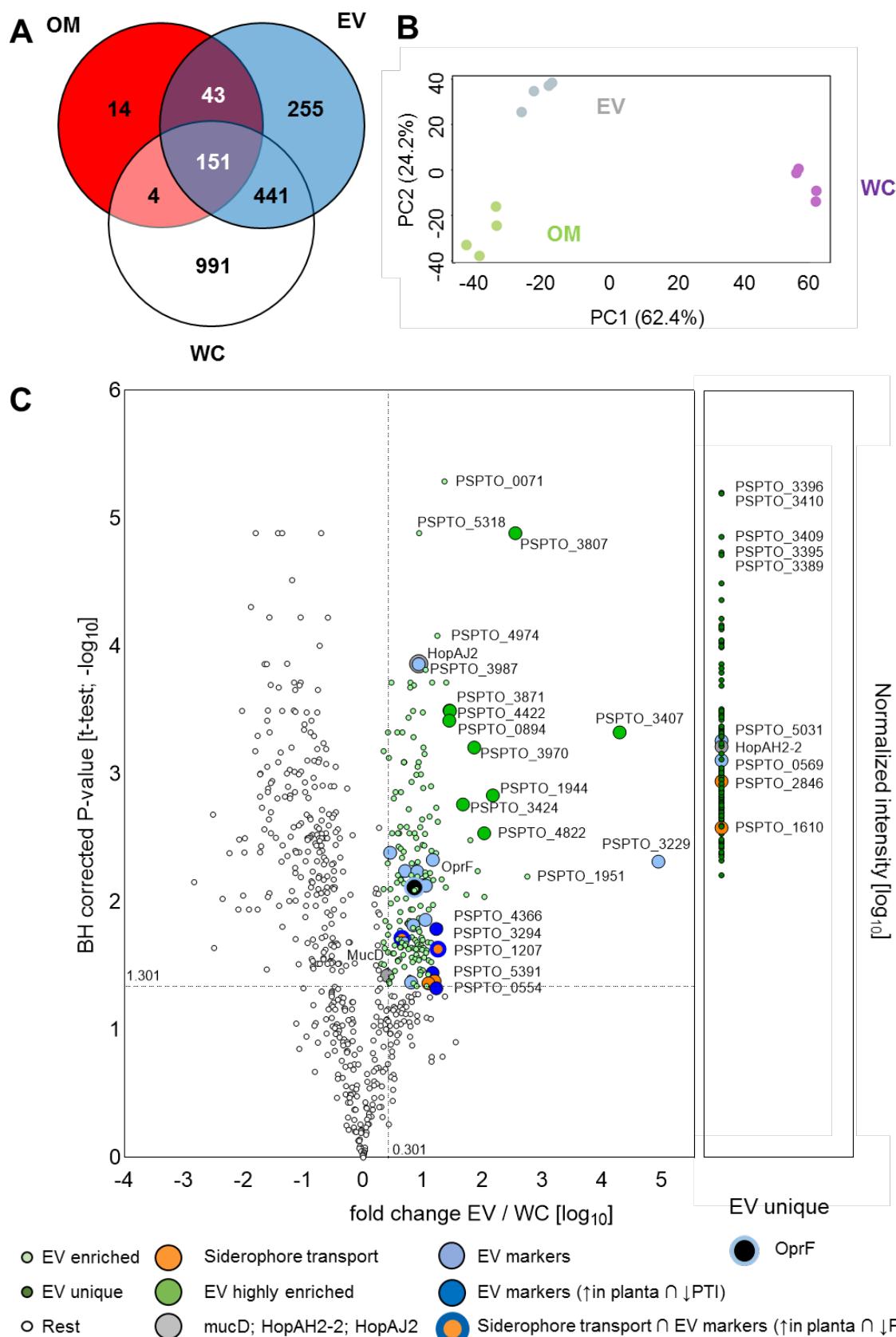
Figure 5. Proteomic analysis identifies 369 proteins enriched in *Pto* DC3000 EVs. A) Comparison of proteins detected in *Pto* DC3000 whole cell lysate (WC), outer membrane (OM) and extracellular vesicles (EV). **B)** Principal Component Analysis (PCA) analysis of

20

identified proteins **C)** Volcano plot comparing EV and WC proteomes. EV-enriched proteins were defined in two categories: I) fold change EV/WC > 2 & FDR < 0.05 (t-test); II) measured in three replicates in EV but not in WC. In addition, the mean intensity in EV protein needs to be in the top 50% of all proteins, so only high intensity proteins in EV are selected. Four types of proteins enriched or unique in EVs were highlighted: proteins related to virulence; proteins related to siderophore transport; candidate EV biomarkers, and proteins highly enriched in EVs compared with WC.

305

306   Next, we performed a gene set analysis on the 369 EV-enriched proteins to examine the

307   biological processes (from gene ontology (GO) (Ashburner *et al.*, 2000, The Gene Ontology,

308   2019) and pathways (KEGG (Kanehisa *et al.*, 2010)), in which these proteins are involved. In

309   total ten GO biological processes were signficantly enriched (FDR < 0,05; DAVID

310   bioinformatics resources (Huang da *et al.*, 2009a, Huang da *et al.*, 2009b)), out of which six

311   were connected with the general process "transport", including transmembrane transport,

312   intracellular transmembrane transport, protein secretion, siderophore transport and protein

313   transport by the Sec complex (Fig. 6B; Table S2). Nine KEGG categories, including cationic

314   antimicrobial peptide resistance, β-lactam resistance and bacterial secretion system are

315   significantly enriched in EVs (Fig. 6B, Table S2).

316

317   We used available *Pto* DC3000 proteome and transcriptome data to examine the *in planta*

318   responses of the EV-enriched proteins (Nobori *et al.*, 2018, Nobori *et al.*, 2020). Comparison

319   with the proteome data showed that of the 369 EV-enriched proteins 78 (21 %) are modulated

320   *in planta* and 48 (13 %) are modulated in immune deficiency mutants (Fig. 6C, Table S3). Of

321   the 369 genes coding for EV-enriched proteins, 98 genes (27 %) were differentially transcribed

322   *in planta* compared to cultured bacteria and 166 genes (45 %) responded to the induction of PTI

323   (Fig. 6D, Table S3). Most EV-unique and EV-highly enriched proteins were transcriptionally

324   upregulated *in planta* whereas the majority of the genes of all identified proteins (WC, OM and

325   EV) were downregulated *in planta* (Fig. 6E). When focussing on GO terms, we found that genes

326   connected with the general process "transport" responded strongly to *in planta* conditions upon

21

327   PTI activation (Fig. 6B). Interestingly, all genes connected with siderophore transport were

328   strongly upregulated in response to *in planta* conditions, but downregulated *in planta* upon

329   activation of PTI (Fig. 6B, Table 1). Thus, during sucessful infection the significant enrichment

330   of siderophore transport proteins at EVs may suggest a role for EVs in iron or other metal ion

331   acquisition (Fig. 5C, orange labelling). When focussing on KEGG pathways, genes connected

332   with protein export (seven out of nine), secretion systems (eight out of eleven), chemotaxis (ten

333   out of twelve) and flagellar assembly (eight out of eight) were affected *in planta* in response to

334   PTI (Fig. 6B).

335
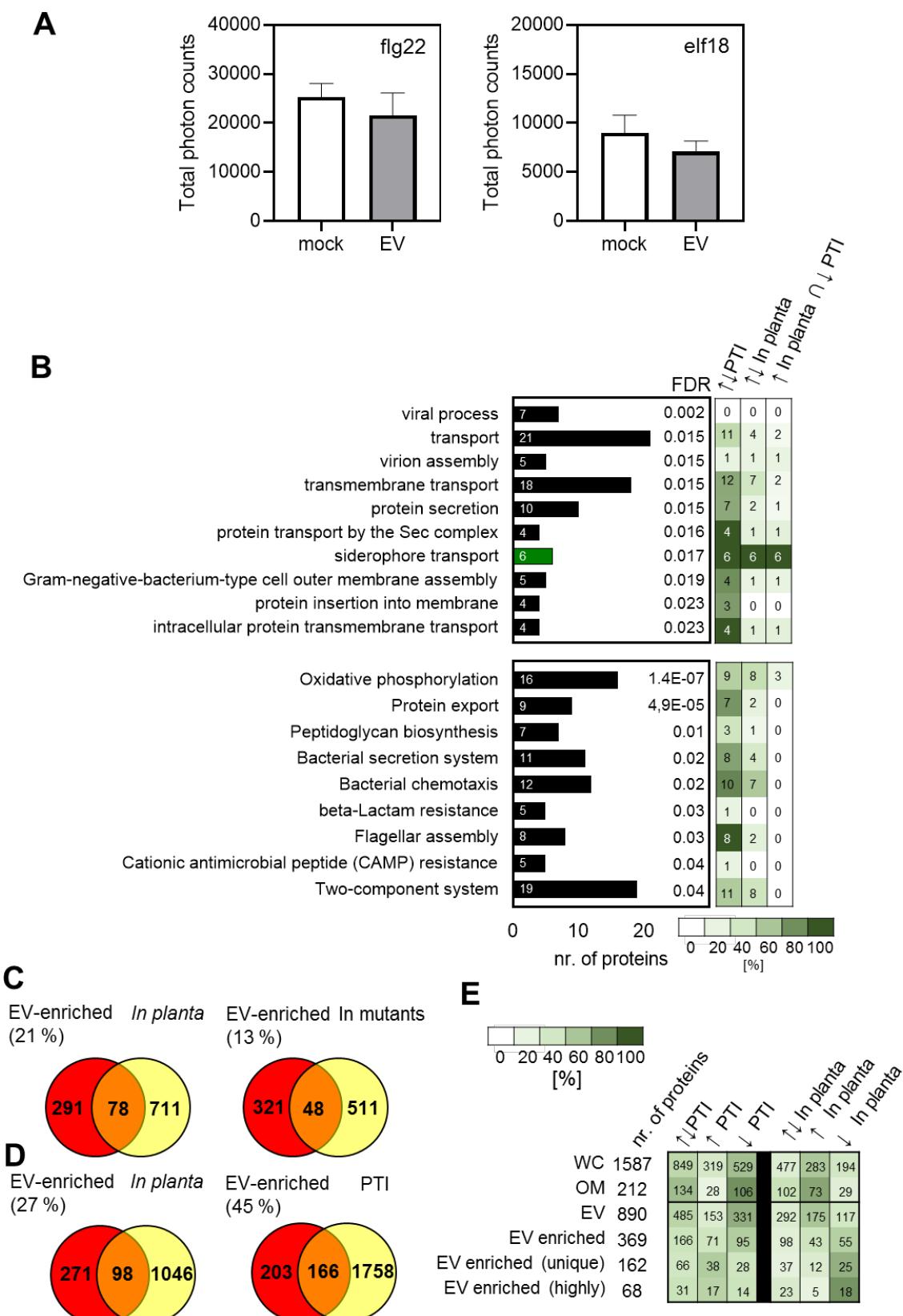
Figure 6. Protein profiles of EVs suggest functions other than classical immune suppression. A) Quantification of MAMP-induced ROS in leaves treated without and with EVs (concentration $\approx 1.10^{10}$) for 24 h. The bars represent mean and error bars represents SEM from n = 12. **B)** Enriched proteins in GO biological processes and KEGG categories in EV-

enriched proteins. The heat-map represents the transcriptional profile based on the comparison of our data with transcriptomic data from (Nobori *et al.*, 2018) of genes encoding proteins identified by GO enrichment analysis. The intensity of green colour represents the percentage of affected genes and numbers in boxes represent the exact number of affected proteins. The arrows indicate transcriptional up- and downregulation. **C)** The Venn diagram represents the number of genes encoding EV-enriched proteins that are transcriptionally regulated *in planta* and responding to immune-deficient *in planta* conditions (Nobori et al. 2020). **D)** Transcriptional regulation of *Pto* DC3000 genes encoding EV-enriched proteins *in planta* and responding to PTI (Nobori *et al.*, 2018). **E)** The heat-map represents the transcriptional regulation of genes encoding identified proteins by proteome analysis *in planta* and responding to PTI (Nobori *et al.*, 2018).

336

Table 1 *In planta* transcription[1] of genes coding proteins enriched in EVs belonging to GO:siderophore transport

Locus tag	Subcellular Localization	Product Description	Gene transcription		other
			*In planta**	PTI**	
PSPTO_1207	Outer Membrane	iron(III) dicitrate transport protein fecA	↑	↓	EV marker
PSPTO_1610	Outer Membrane	TonB-dependent siderophore receptor	↑	↓	EV unique
PSPTO_2152	Outer Membrane	TonB-dependent siderophore receptor	↑	↓	
PSPTO_2846	Outer Membrane	TonB-dependent siderophore receptor	↑	↓	EV unique
PSPTO_3294	Outer Membrane	TonB-dependent siderophore receptor	↑	↓	EV marker
PSPTO_3574	Outer Membrane	TonB-dependent siderophore receptor	↑	↓	

[1] Nobori et al. 2018. Increased (↑) or decreased (↓) gene transcription *in planta* vs *in vitro** or under induced PTI *in planta* vs non-induced PTI *in planta***.

337

Pto DC3000 appears to release EVs in the form of OMVs and OIMVs

Classification of the proteins enriched in EVs by putative subcellular localization revealed distinct localization profiles compared with WC and OM proteins. While 66 % of WC proteins were cytoplasmic, about half (51 %) of the EV-enriched proteins were cytoplasmic membrane-associated, with the next largest known class being OM-associated (11 %) (Fig. 7A). Yet, being putative localizations, we cannot exclude the possibility of other/additional localizations of the proteins as currently predicted, in particular for anchor-less proteins. Because the localization profile of the EV-enriched protein suggested that *Pto* DC3000 produces EVs in the form of OIMVs (Perez-Cruz *et al.*, 2015), we performed additional transmission electron microscopy (TEM) analysis of *Pto* DC3000 bacteria. Micrographs of the sectioned samples showed several structures reminiscent of budding vesicles from the bacterial outer membrane (Fig. 7B, 7C). Combining the data from proteomics and TEM, it may suggest that *Pto* DC3000 produces EVs

350   in the form of both OMVs and OIMVs, as previously described for the closely related species

351   *Pseudomonas aeruginosa* (Toyofuku *et al.*, 2019).
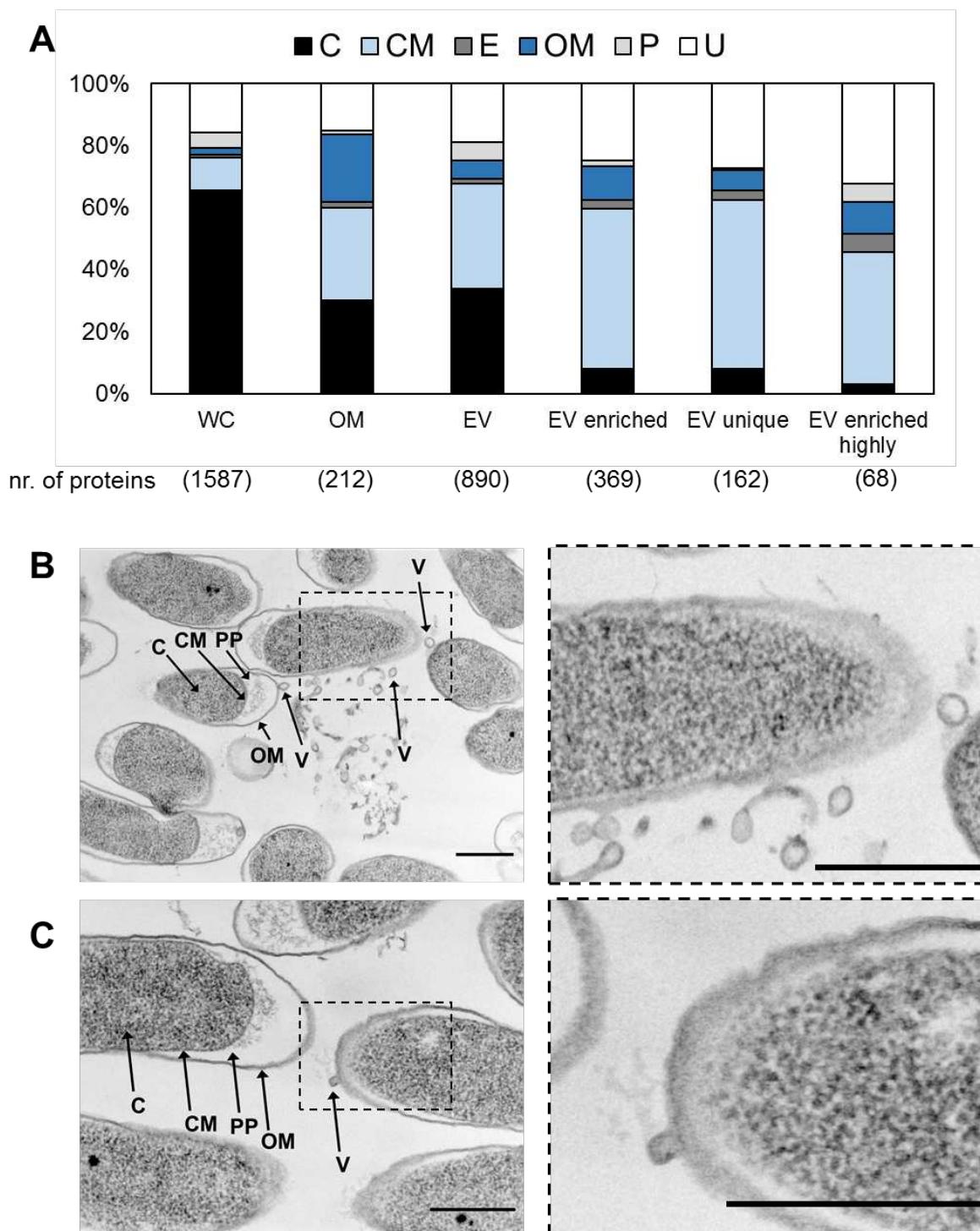
Figure 7. Localization profiles of EV proteins and TEM analysis suggest the release of *Pto* DC3000 EVs in the form of OMVs and OIMVs. A) Predicted protein localization of identified in whole cell lysate (WC), outer membrane (OM), EVs, EV-enriched, EV unique (the proteins identified only in EVs not in WC) and EV enriched – highly (protein which FDR < 0.005 and EV/WC > 20) in [%]. **B-C)** The left panel shows representative TEM micrographs from planktonic *Pto* DC3000 cultures (OD_{600} = 3-4). C, cytoplasm; CM,

cytoplasmic membrane; OM, outer membrane; PP, periplasm; V, vesicle. All scale bars = 500 nm. **B)** A lot of smaller and larger vesicles in proximity to cells. It is important to note that the larger vesicle-like structures could also represent debris of death cells. **C)** Budding vesicle in the right part of the micrograph. Dashed boxes indicate enlarged regions of the micrographs shown in the right panel.

352

353 **Comparative analysis of proteomic data revealed 20 candidates for *Pto* DC3000 EVs**

354 **markers**

355 Since a number of EV proteomes have been reported from *P. aeruginosa* (Couto N. *et al.*, 2015,

356 Choi *et al.*, 2011, Reales-Calderon *et al.*, 2015), we addressed whether the protein composition

357 of EVs from *Pto* DC3000 and *P. aeruginosa* PAO1 (*Pa* PAO1) share similarities. We focussed

358 on three published *Pa* PAO1 EV proteomes and found that 103 proteins were identified in the

359 EV proteomes across the three reports (Couto N. *et al.*, 2015, Choi *et al.*, 2011, Reales-Calderon

360 *et al.*, 2015). Of the 103 shared EV proteins from *Pa* PAO1, we could identify 100 orthologous

361 proteins encoded in the *Pto* DC3000 genome and 44 proteins were enriched in *Pto* DC3000

362 EVs (Table S4). We refer to these as the EV "core". These proteins were highly enriched in

363 localization to the outer membrane (44 %) and cytoplasmic membrane (26 %) (Fig. 8A),

364 consistent with EVs released in the form of OMVs (Fig. 7B, 7C). From these 44 proteins, 20

365 were putative outer membrane-localized proteins and thus represent good candidate biomarkers

366 for the detection of EVs (Table 2, S4; Fig. 5C blue labelling). Interestingly, 20 out of 31 proteins

367 with predicted membrane localization (20 out of 31) were transcriptionally regulated *in planta*

368 in response to PTI activation (Nobori *et al.*, 2018), of which 14 showed downregulation.

369 Overall, twelve of the 31 proteins responded transcriptionally to the *in planta* condition, with

370 nine showing upregulation (Fig. 8B).

371

372 One of the predicted EV markers is OprF (Outer membrane porin OprF; Fig. 5C black

373 labelling), which we used for immunodection of *Pto* DC3000 EVs *in planta* and purified from

374 *Pto* DC3000 cultures. Using *anti*-OprF antibodies, we identified specific bands in filtered

26

375   apoplastic fluids of *A. thaliana* leaves infected with *Pto* DC3000 at two and three days post

376   infection but not in control treated plants (Fig. 8C). This provides additional evidence that *Pto*

377   DC3000 releases EVs *in planta* during infection.

378
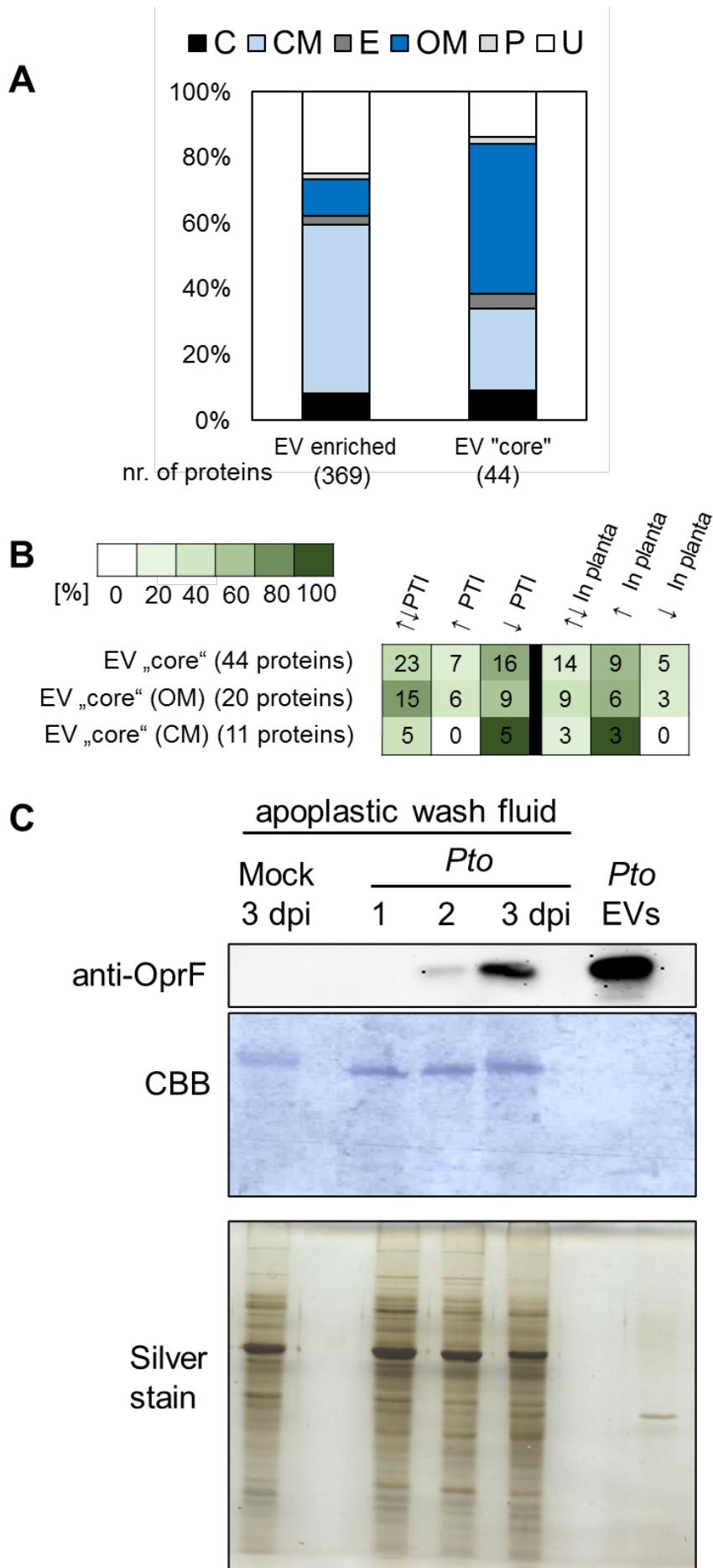
Figure 8. Prediction of Pseudomonas "core" EVs proteins identifies biomarkers for the detection of *Pto* DC3000 EVs *in planta*. A) Predicted protein localization of the *Pto* DC3000 EV enriched proteins whose orthologs are found in *P. aeruginosa* EV proteomes [%] total number of identified proteins is 44. **B)** Heat-map representing transcriptional changes in genes encoding *Pseudomonas* "core" EV proteins, EV "core" proteins localized on outer membrane (OM) and EV "core" proteins localized on cytoplasmic membrane (CM). The intensity of green colour represents percentage of affected genes and the numbers in boxes show the exact number of affected genes. **C)** Immunoblot monitoring OprF, a predicted *Pto* DC3000 EV biomarker, in EVs collected from apoplastic fluids. OprF antibodies detect bands in apoplastic fluids from *A. thaliana* infected with *Pto* DC3000 and in gradient enriched EVs. Coomassie Brilliant Blue (CBB) and silver staining are shown as loading control.

379

380

29

Table 2 *In planta* transcription[1] of genes coding proteins suggested as promising candidates to be EV markers

Locus Tag	UniProt ID	Subcellular Localization	Name	Gene expression		other
				PTI*	In planta**	
PSPTO_0554	Q88A43	Outer Membrane	organic solvent tolerance protein	↓	↑	
PSPTO_0569	Q88A28	Outer Membrane	autotransporting lipase, GDSL family	↑	n.s.	EV unique
PSPTO_1207	Q887S9	Outer Membrane	iron(III) dicitrate transport protein fecA	↓	↑	Siderophore transport
PSPTO_1296	Q887J6	Outer Membrane	porin B	↑	n.s.	
PSPTO_1437	Q886Y7	Outer Membrane	lysyl-tRNA synthetase	↓	n.s.	
PSPTO_1542	Q886N5	Outer Membrane	outer membrane protein	↓	n.s.	
PSPTO_1720	Q885W1	Outer Membrane	outer membrane protein	↑	↓	
PSPTO_2272	Q883S8	Outer Membrane	outer membrane lipoprotein OprI	n.s.	↓	
PSPTO_2299	Q883Q1	Outer Membrane	outer membrane porin OprF	n.s.	↑	
PSPTO_3229	Q880E1	Outer Membrane	filamentous hemagglutinin, intein-containing	↑	↓	
PSPTO_3294	Q87ZX8	Outer Membrane	TonB-dependent siderophore receptor	↓	↑	Siderophore transport
PSPTO_3971	Q87Y41	Outer Membrane	peptidoglycan-associated lipoprotein	n.s.	n.s.	
PSPTO_3987	Q87Y25	Outer Membrane	porin D	n.s.	n.s.	beta-Lactam resistance
PSPTO_4115	Q87XR1	Outer Membrane	lipoprotein SlyB	↑	n.s.	
PSPTO_4366	Q87X24	Outer Membrane	iron-regulated protein A	↓	↑	
PSPTO_4839	Q87VU6	Outer Membrane	hypothetical protein	↑	n.s.	
PSPTO_4940	Q87VJ6	Outer Membrane	hflK protein	↓	n.s.	
PSPTO_4977	Q87VG0	Outer Membrane	outer membrane efflux protein TolC	↓	n.s.	Bacterial secretion system; beta-Lactam resistance; Cationic antimicrobial peptide (CAMP) resistance
PSPTO_5031	Q87VA8	Outer Membrane	type IV pilus biogenesis protein PilJ	n.s.	n.s.	EV unique
PSPTO_5391	Q87UB4	Outer Membrane	outer membrane porin, OprD family	↓	↑	

[1] Nobori et al. 2018. Increased (↑) or decreased (↓) gene transcription *in planta* vs *in vitro** or under induced PTI *in planta* vs non-induced PTI *in planta***. n.s. = non-significant

Discussion

Bacterial EVs have been widely studied for their content and biological importance in various human diseases. Until recently, however, EV production by phytopathogenic bacteria has been mostly disregarded (Rybak & Robatzek, 2019). In the past few years, the attention in plant-microbe interactions has turned slowly towards EV signalling. EV production by phytopathogenic bacteria was shown for *A. tumefaciens* C58, *Xanthomonas campestris* pv *campestris* (*Xcc*), *X. campestris* pv *vesicatoria*, *Pto* T1, *Pto* DC3000 and *Xyllela fastidiosa* subsp. *fastidiosa* Temecula-1, subsp. *pauca* 9a5c and subsp. Fb7 (Bahar *et al.*, 2016, Feitosa-Junior *et al.*, 2019, Chowdhury & Jagannadham, 2013, Ionescu *et al.*, 2014, Knoke *et al.*, 2020, McMillan *et al.*, 2020, Sidhu *et al.*, 2008, Sole *et al.*, 2015). In this study, we provide several pieces of evidence for the role of EVs in the interaction of *Pto* DC3000 with plants: i) the bacteria produce EVs *in planta* during infection; ii) proteins responding to the plant environment are enriched in EVs; iii) known MAMPs and effectors are associated with EVs; and iv) plants respond to EVs with prototypic PTI reactions.

We show that *Pto* DC3000 produces spheres bulging from its outer membrane and releases spherical vesicles into the environment (Fig. 1A, 7B, 7C). Our data indicate the production of EVs predominantly in the form of OMVs albeit the predicted localization profiles of the EV-enriched proteins also suggest OIMV production (Fig. 7A, 7B, 7C, 8A), both representing well-established routes of vesicle release in Gram-negative bacteria (Toyofuku *et al.*, 2019). The more polydisperse size seen for EVs recovered from apoplastic fluids of susceptible *Pto* DC3000 infected plants could not only represent a mixed pool of plant and bacterial derived EVs, but also suggests that *Pto* DC3000 might release EVs from different biogenesis routes including membrane blebbing and explosive cell lysis.

31

406 Our results suggest the regulated production of EVs and the specific enrichment of proteins to

407 EVs. *Pto* DC3000 cultures produced more EVs with increasing bacterial density during

408 exponential-phase growth, showing a correlation between bacteria and EV numbers (Fig. 1E).

409 The production of EVs by *Pto* DC3000 was slightly responsive to bacterial growth style and

410 isolation technique. EVs produced from biofilm *Pto* DC3000 and fluid planktonic culture were

411 smaller and more negatively charged than gradient enriched planktonic EVs. Moreover, heat

412 inactivation of bacteria increased vesicle numbers and size (Fig. 1D, 1F). Since EVs from heat

413 inactivated bacteria did not differ in charge profiles compared to untreated EVs (Fig. S6D), it

414 is possible that explosive cell lysis contributes to the higher EV numbers (Toyofuku *et al.*,

415 2019). Turnbull *et al*. demonstrated that explosive cell lysis of a sub-population of cells from *P.*

416 *aeruginosa* biofilms results in the generation of bacterial EVs (Turnbull *et al.*, 2016).

417 Furthermore, heat shock stimulates the release of OMVs, most likely a result of high levels of

418 un- and misfolded proteins accumulating in heat-stressed cells (Macdonald & Kuehn, 2013,

419 McBroom & Kuehn, 2007). In this context it is interesting to note that the biophysical

420 characteristics of *Pto* DC3000 EVs remained largely unchanged under disruptive treatment

421 conditions except boiling (Fig. 2). Thus, the EVs from *Pto* DC3000 are stable and can maintain

422 functionality as reported previously for other bacteria (Alves *et al.*, 2016, Arigita *et al.*, 2004,

423 Frank *et al.*, 2018).

424

425 A range of activities has been associated with bacterial EVs. This includes modulation of host

426 immunity i.e. through EVs presenting MAMPs and delivering effector molecules (Bahar *et al.*,

427 2016, Schwechheimer & Kuehn, 2015). We found that EVs from *Pto* DC3000 cultures elicited

428 a robust induction of the *FRK1* defence marker gene (Fig. 4B, 4C, 4E). Compared with EVs

429 from *Acidovorax* and *Xanthomonas* bacteria, *Pto* DC3000 EVs provoked a modest induction of

430 defence gene expression (Bahar *et al.*, 2016). Despite this, the *Pto* DC3000 EVs did not trigger

32

431   a growth arrest in Arabidopsis seedlings (Fig. 4D). These results suggest that the immunogenic

432   activities of the EVs, but not a longer-term trade-off with growth, may be relevant in their

433   interaction with plants. In contrast to our results, McMillan et al. reported significant seedling

434   growth repression in response to *Pto* DC3000 EVs (McMillan *et al.*, 2020). This disparity in

435   results may be due to several factors, including differences in the growth conditions of both the

436   bacterial cultures and the *A. thaliana* seedlings, the type of biochemical isolation of EVs and

437   vesicle dose. That EVs can serve as protective vaccines has been reported for many bacteria but

438   not phytopathogens. We show here that plants pre-treated with *Pto* DC3000 EVs were modest,

439   yet significantly protected against subsequent infection with *Pto* DC3000 bacteria (Fig. 4A).

440   Consistently, EV pre-treatments did not inhibit a MAMP-induced ROS burst (Fig. 6A). The

441   stronger protective immune response observed by McMillan et al. may be due to differences in

442   experimental procedures, as noted above (McMillan *et al.*, 2020). In addition, McMillan et al.

443   showed that pre-treatment with bacterial EVs provided protection against subsequent oomycete

444   infection (McMillan *et al.*, 2020). The potential for *Pto* DC3000 EVs to induce broad-spectrum

445   resistance supports a role for PTI.

446

447   PTI   responses   to *Pto*   DC3000   involve   recognition   by   FLS2,   EFR   and   LIPO-

448   OLIGOSACCHARIDE-SPECIFIC   REDUCED   ELICITATION   (LORE),   which   detect

449   immunogenic   flg22,   elf18   and   3-OH-FAs   (Wan   *et   al.*,   2019).   EVs   from   bacterial

450   phytopathogens are enriched in EF-Tu and LPS (Bahar *et al.*, 2016, Feitosa-Junior *et al.*, 2019,

451   Sidhu *et al.*, 2008), suggesting the presence of elf18 and 3-OH-FAs. Bahar *et al.* demonstrated

452   that   BRI1-ASSOCIATED   KINASE   1   (BAK1)   and   SUPPRESSOR   OF   BIR   1   (SOBIR1),

453   interacting   co-receptors   of   PRRs,   mediate   the   immunogenic   perception   of   EVs   from *X.*

454   *campestris* pv. *campestris* (Bahar et al., 2016). We show that our vesicle samples from *Pto*

455   DC3000 elicit immune responses that are dependent on FLS2 (Fig. 4E). Despite depleting

33

456 extracellular components from EV samples by density gradient centrifugation, it is possible that

457 flagella co-purify with the *Pto* DC3000 EV samples, since filamentous structures were observed

458 in SEM analysis (Fig. 1B). Contamination of flagella in EVs was reported to contribute to the

459 detection of FliC in EVs from *P. aeruginosa* (Bauman & Kuehn, 2006). However, flagella

460 proteins such as FliC have a specific affinity for EVs and are involved in EV production in

461 *Escherichia coli* (Manabe et al., 2013). We cannot exclude that flagella proteins play roles in

462 EV production in *Pto* DC3000, evidenced by the finding that six flagella-associated proteins

463 were enriched in *Pto* DC3000 EVs (Table S1).

464

465 Why *Pto* DC3000 produces EVs during infection is unclear. It is evident that the plant apoplast

466 represents a stressful environment for its colonizing bacteria. Bacteria respond to environmental

467 stress with the production of EVs, which allows for cell surface remodelling, secretion of

468 degraded and damaged cargo, and uptake of nutrients in bacterial communities i.e. by packaging

469 transporters in EVs (Schwechheimer & Kuehn, 2015, Toyofuku *et al.*, 2019, Zingl *et al.*, 2020).

470 As the growth state of bacteria determines the nutrient availability, the production of EVs could

471 support the growth of *Pto* DC3000 in culture and *in planta*. Proteomics analysis of gradient

472 enriched *Pto* DC3000 EVs identified 890 vesicle-associated proteins, of which 369 were

473 enriched in the EVs relative to the cellular proteome (Fig. 5, Table S1). The mechanisms by

474 which this enrichment occurs suggests a selective delivery of cargo into the EVs and should be

475 investigated in the future. Of the EV-enriched proteins, six out of ten GO biological process

476 categories were related to transport mechanisms (Fig. 6B). Proteins involved in siderophore

477 transport were enriched in the EVs and have recently been shown to play a role in *Pto* DC3000

478 infection success (Nobori *et al.*, 2018). Interestingly, the expression of genes coding for all

479 siderophore transport proteins enriched in EVs was upregulated *in planta* compared to *in vitro*

480 conditions as well as downregulated upon induction of PTI (Fig. 6B; Table 1) (Nobori *et al.*,

481 2018). Thus, regulation of siderophore transport proteins can be considered as an adaptive

482 response of *Pto* DC3000 to iron/metal ion availability, and secretion into EVs may allow

483 improved acquisition of iron, analogous to EV secretion of the siderophore mycobactin in

484 *Mycobacterium tuberculosis* (Prados-Rosales et al., 2014). The plant's apoplast, which is the

485 niche colonized by *Pto* DC3000 represents an environment where bacteria are challenged with

486 iron acquisition and plant defence molecules (Nobori *et al.*, 2018). The role of bacterial EVs in

487 metal acquisition is not restricted to iron. *Neisseria meningitidis* produces OMVs, which are

488 enriched in zinc acquisition proteins (Lappann *et al.*, 2013), and zinc regulates siderophore

489 biosynthesis genes in *Pseudomonas fluorescens* (Rossbach et al., 2000). It is thus feasible that

490 *Pto* DC3000 produces EVs to help it adapt to metal conditions in the environment including the

491 plant's apoplast.

492

493 The hypothesis that *Pto* DC3000 uses EVs to adapt to the growth environment is supported by

494 our finding that *Pto* DC3000 EVs are enriched in proteins related to the KEGG categories β-

495 lactam resistance and cationic antimicrobial peptide resistance (Fig. 6B). Several studies

496 demonstrated that EVs can improve bacterial survival during antibiotic exposure.

497 *Stenotrophomonas maltophilia* produced more EVs upon treatment with the β-lactam antibiotic

498 imipenem (Devos *et al.*, 2015, Devos *et al.*, 2017). Its EVs contained β-lactamase and increased

499 *S. maltophilia* survival in the presence of antibiotics (Devos *et al.*, 2017). Plants defend

500 infection by upregulation of many defence-related gene including genes coding for

501 antimicrobial peptides (Campos *et al.*, 2018). It is possible that *Pto* DC3000 produces EVs to

502 counter the action of plant-derived antimicrobial peptides. Collectively, we propose that *Pto*

503 DC3000 produces EVs to improve its growth capacity both in culture and *in planta*. These

504 findings should stimulate further studies on the role of EVs in the interaction of bacteria with

505 plants, for example identifying the composition of EVs *in planta* using biomarkers.

506

Experimental procedures

Bacterial strains and growth

Pseudomonas syringae pv. *tomato* DC3000 (*Pto* DC3000) used in this study were routinely cultured at 28 °C in King's B medium containing 50 µg/mL Rifampicin at 180 rpm and on plates with 1% agar without agitation. Planktonic growth was performed in 500 mL and growth rates were measured over time as OD_{600}. Biofilm growth was measured after 24 h on plate, transferring all bacteria per plate in 10 mL 0.85% saline.

Plant material and growth conditions

Arabidopsis thaliana ecotype Columbia (Col-0), *pFRK1*::GUS (Kunze et al. 2004), *fls2c* (Zipfel et al. 2004) and *efr-1* (Zipfel et al. 2006) mutants were used in this study. For bacterial infections and ROS assays, Col-0 plants were soil-grown at 21–22 °C and 8 h photoperiod. For GUS assays, RT-qPCR analysis and induced growth arrest, seedlings were sterile grown on Murashige and Skoog (MS) plates supplemented with 1% sucrose and 1.5% gelrite (Duchefa, Netherlands) pH 5.8 for four days (after 2-4 days stratification in the dark at 4 °C), then transferred to 96-well plates containing 150 µL ½ MS medium supplemented with 1% sucrose per well and grown for eleven to twelve days in at 22 °C and 16 h photoperiod ($120 - 150$ µE.m^{-2}.s^{-1}).

Extraction and purification of bacterial EVs

EVs were routinely isolated from planktonic cultures at early-logarithmic to late-stationary phases as well as biofilm cultures (Fig. S2B, S2D). 100 mL of planktonic grown bacteria and 10 mL of biofilm grown bacteria, respectively, were pelleted at 4,500 x g for 2 x 20 min, the supernatant was decanted and passed through a 0.22 µm membrane (fluid samples; Fig. S2A).

531   Particles were pelleted from the cell-free supernatant at 100,000 x g for 1.5 h. The pellet was

532   resuspended in 1.7 mL 1mM EDTA and loaded on sucrose density step-gradient (1.7 mL of

533   sucrose 25%, 35%, 45%, 50%, 55%) and centrifuged at 160,000 x g for 18 h. 2 mL samples

534   were collected from each of the sucrose density steps and diluted with 1 mM EDTA to 30 mL.

535   Particles were pelleted at 100,000 x g for 2 h and the pellets were each resuspended in 0.16 mL

536   1 mM EDTA (gradient enriched samples; Fig. S2A). EV samples were immediately frozen in

537   liquid nitrogen. Since most EVs migrated to the 55% density fraction (Fig. S6A), we then

538   collected EVs across fractions 3 to 5, which were less variable in ζ-potential and size compared

539   to fractions 1 and 2 (Fig. S6B, S6C).

540

541   **Extraction of leaf apoplastic fluids**

542   Apoplastic fluids were collected from leaves of six to seven weeks old plants. The leaves were

543   cut of the rosette and vacuum infiltrated with particle-free 1 mM EDTA. After removing excess

544   buffer, infiltrated leaves were placed into 20 mL syringes and centrifuged in 50 mL conical

545   tubes at 900 x g for 20 minutes at 4°C. The resulting apoplastic wash was passed through a 0.22

546   μm membrane (apoplastic fluid samples).

547

548   **EV quantification, size and charge measurements**

549   EVs were quantified, size and charge measured by Nanoparticle Tracking Analysis (NTA)

550   using ZetaView® BASIC PMX-120 (Particle Metrix, Germany) at room temperature. To detect

551   EVs, we used the manufacturer's default settings for liposomes. Particle quantification and size

552   measurements were performed by scanning eleven cell positions each and capturing 30 frames

553   per position with the following settings: Focus: autofocus; Camera sensitivity for all samples:

554   85; Shutter: 100; Scattering Intensity: detected automatically. After capture, the videos were

555   analysed by the in-built ZetaView Software 8.05.11 [ZNTA] with the following specific

556   analysis parameters: Maximum area: 1000, Minimum area 5, Minimum brightness: 25,

557   Tracelength: 15 ms. Hardware: embedded laser: 40 mW at 488 nm; camera: CMOS. For particle

558   charge measurements, the same settings were used except Minimum brightness: 30. Statistical

559   analysis was performed using either One-way ANOVA with Tukey post hoc test or Welsch´s

560   ANOVA with Dunnett´s T3 multiple comparisons post hoc test.

561

562   All samples were diluted in particle-free 1 mM EDTA buffer, checked with NTA.

563   Unconditioned King's B medium contained up to 1.4×10^9 particles (Fig. 1D). *Pto* DC3000

564   cultures contained increasing particles numbers with cultivation time: $\approx 2.8 \times 10^9$ particles at

565     $OD_{600} = 3\text{-}4$ (50% of influence); $\approx 3.7 \times 10^9$ particles at $OD_{600} = 4.5\text{-}5.5$ (37% of influence), $\approx$

566   7×10^9 particles at OD_{600} 7.5-9 (20% of influence), and $\approx 1.1 \times 10^{10}$ particles at OD_{600} 10 -11

567   (13% of influence) (Fig. 1D). We therefore focused our measurements on samples collected

568   from $OD_{600} > 7.5$, which shows lower than 20% influence of particles from the medium (Fig.

569   1D), as well as calculated EV concentrations to the colony forming units (CFU) of the bacterial

570   cultures.

571

572   **Scanning electron microscopy**

573   Planktonic grown bacteria at $OD_{600} = 3\text{-}4$ and gradient enriched EVs (0.5 to 1.5×10^{10} particles)

574   were used for scanning electron microscopy (SEM). The cells were chemically fixed using 2.5%

575   glutaraldehyde in 50 mM cacodylate buffer (pH 7.0) containing 2 mM $MgCl_2$. Then the cells

576   were applied to a glass slide, covered with a cover slip and plunge frozen in liquid nitrogen.

577   After this, the cover slip was removed and the cells were place in fixation buffer again. After

578   washing 4 times with buffer, post-fixation was carried out with 1% OsO_4 for 15 min. Two

579   additional washing steps with buffer were followed by three times washing with double distilled

580   water. The samples were dehydrated in a graded acetone series, critical-point-dried and

581   mounted on an aluminium stub. To enhance conductivity, the samples were sputter-coated with

582   platinum. Microscopy was carried out using a Zeiss Auriga Crossbeam workstation at 2 kV

583   (Zeiss, Oberkochen, Germany). The vesicle size was manually measured across five randomly

584   selected SEM micrographs using Fiji software (Schindelin *et al.*, 2012).

585

586   **Transmission electron microscopy**

587   Planktonic grown *Pto* DC3000 at OD_{600} = 3-4 were used for ultrathin sectioning and subsequent

588   transmission electron microscopy (TEM). The cells were concentrated by centrifugation and

589   the cells were high-pressure frozen using a Leica HPM100 (Leica Microsystems, Wetzlar,

590   Germany). This was followed by freeze-substitution with 0.2% osmium tetroxide, 0.1% uranyl

591   acetate, 9.3% water in water-free acetone in a Leica AFS 2 (Leica Microsystems, Wetzlar,

592   Germany) as described previously (Flechsler *et al.*, 2020). After embedding in Epon 812

593   substitute resin (Fluka Chemie AG, Buchs Switzerland), the cells were ultrathin sectioned (50

594   to 100 nm thickness) and post-stained for 1 min with lead citrate. Transmission electron

595   microscopy of ultrathin sections was carried out with a JEOL F200 cryo-S(TEM), which was

596   operated at 200 kV and at room temperature in the TEM mode. Images were acquired using a

597   bottom-mounted XAROSA 20 mega pixel CMOS camera (EMSIS, Münster, Germany).

598

599   ***Pto* DC3000 infection assay**

600   Overnight plate-grown *Pto* DC3000 cells were resuspended in 10 mM $MgCl_2$ and diluted to

601   OD_{600} = 0.0006. Using a needle-less syringe, the bacterial suspension was infiltrated into mature

602   leaves of five to six weeks old plants, three leaves per plant. For pre-treatments, , gradient

603   enriched EVs from planktonic *Pto* DC3000 (concentration $\approx 1.10^{10}$), and 0.02 mM EDTA as a

604   negative control and 100 nM flg22 (EZbiolabs) as a positive control were syringe-infiltrated

605   into leaves 24 h prior *Pto* DC3000 inoculation. Discs of the infected leaves (one disc per leaf,

606   0.6 cm diameter) were excised at one, two- or three-days post infection (dpi). The three leaf

607   discs from each plant were pooled and ground in 1 mL 10 mM $MgCl_2$. Serial dilutions were

608   plated on LB medium with rifampicin (50 µg/mL) and bacterial colonies were counted one day

609   after incubation at 28 ºC. Statistical analysis was performed using two tailed Welsch´s t-test.

610

611   **Histochemical β-glucuronidase (GUS) staining**

612   The histochemical GUS assay was performed with eleven day old seedlings. Seedlings were

613   treated with gradient enriched *Pto* DC3000 EVs (concentration $\approx 1.10^{10}$), 100 nM flg22

614   (EZbiolabs) or as a control with 0.02 mM EDTA for 18 h. Treated seedlings were immersed in

615   X-Gluc buffer [2 mM X-Gluc (Biosynth), 50 mM $NaPO_4$, pH 7, 0.5 % (v/v) Triton-X100, 0.5

616   mM K-ferricyanide] for 16 h at 37 °C. Chlorophyll was removed by repeated washing in 80 %

617   (v/v) ethanol. Observations were made on a WHX 6000 digital microscopy (Krckova *et al.*,

618   2018).

619

620   **Fluorimetric GUS assay**

621   For fluorimetric GUS assays, eleven to twelve days old seedlings were treated with gradient

622   enriched *Pto* DC3000 EVs (concentration $\approx 1.10^{10}$) or with 100 nM flg22 (EZbiolabs) or as a

623   control with 0.02 mM EDTA for 18 h. Treated seedlings were frozen in liquid nitrogen in 2 mL

624   conical tubes containing 2 clean sterile glass beads and liquid nitrogen. The frozen samples

625   were dry homogenized using a Retch mixer mill (Retch). Homogenized samples were kept on

626   ice and cold (4 °C). For total protein extraction, GUS extraction buffer was added as described

627   (Andriankaja *et al.*, 2007) [50 mM sodium phosphate (pH 7); 10 mM 2-mercaptoethanol; 10

628   mM Na_2EDTA; 0.1% Triton X-100; 0.1% sodium lauryl-sarcosine and PPIC]. GUS activities

629   were measured fluorimetrically in reaction buffer (see below) using Methylumbelliferyl-β-D-

630   glucuronic acid dihydrate (MUG), (Biosynth) as a substrate. Reaction buffer was the same

631   solution as extraction buffer with one modification: PPIC was replaced by 1 mM MUG. The

632   fluorescence was measured using TECAN fluorimeter at excitation 360 nm and emission 465

633   nm. The enzymatic activity of the sample was calculated to protein concentration measured by

634   Bradford protein assay. The absorbance was measured using TECAN spectrometer absorbance

635   at 595 nm. Statistical analysis was performed using One-way ANOVA with Tukey post hoc

636   test.

637

638   **RNA extraction and RT-qPCR analysis**

639   Gene transcription analysis was performed with twelve days old seedlings. The seedlings were

640   treated with gradient enriched EVs (concentration 1.10^{10}) and 0.02 mM EDTA as control for 3

641   h, frozen in liquid nitrogen and ground with 2.5-mm diameter silica beads using a homogenizer

642   (Retch, Germany). Total RNA was isolated using a TRIzol® reagent (Invitrogen, USA)

643   according to the manufacturer's protocol. The extracted RNA was treated with a DNA-free kit

644   (Ambion, USA). Subsequently, 1 μg of RNA was converted into cDNA with M-MLV RNase

645   H– Point Mutant reverse transcriptase (Promega Corp., USA) and an anchored oligo dT21

646   primer (Metabion, Germany). Gene transcription was quantified by qPCR using a LightCycler

647   480 SYBR Green I Master kit and LightCycler 480 (Roche, Switzerland). The PCR conditions

648   were 95 °C for 10 min followed by 45 cycles of 95 °C for 10 s, 55 °C for 20 s, and 72 °C for

649   20 s. Melting curve analyses were then carried out. Relative transcription was normalized to the

650   housekeeping gene *AtTIP41* (Czechowski *et al.*, 2005). Primers were designed using PerlPrimer

651   v1.1.21 (Marshall, 2004). The primers used are *AtFRK1*_FP, GCCAACGGAGACATTAGAG;

652   *AtFRK1*_RP, CCATAACGACCTGACTCATC. Statistical analysis was performed using One-

653   way ANOVA with Tukey post hoc test.

654

655   **Seedling growth analysis**

656   Four days old seedlings were transferred from MS solid media into the liquid MS media in

657   transparent 96-well microplates. Each well contained 100 μL of media either containing 0.02

658   mM EDTA as a control or gradient enriched *Pto* DC3000 EVs (concentration $\approx 1.10^{10}$) or with

659   100 nM flg22 (EZbiolabs) as a positive control. After eight days, the treated seedlings were

660   dried using paper towel and then the fresh weight was measured. Based on the weight of each

661   seedling relative seedlings growth [%] to control seedlings was calculated. Statistical analysis

662   was performed using Welsch´s ANOVA with Dunnett´s T3 multiple comparisons post hoc test

663   two tailed Student t-test.

664

665   **ROS measurements**

666   ROS production was determined using the luminol-based assay as previously described

667   (Mersmann *et al.*, 2010). Briefly, leaves of five to six weeks old *A. thaliana* plants were

668   infiltrated with gradient enriched EVs (concentration $\approx 1.10^{10}$). After 2 h, discs were excised

669   from the infiltrated leaves and 24 h incubated in ddH$_2$O at 22 °C. Then, the leaf discs were

670   treated with 100 nM flg22 or 100 nM elf18 (EZbiolabs) to induce the production of ROS. The

671   total photon count was collected for 45 min using a TECAN luminometer. Statistical analysis

672   was performed using two tailed Student t-test.

673

674   **Proteomics**

675   We isolated proteins from *Pto* DC3000 whole cell lysates (WC) (Park *et al.*, 2014) and outer

676   membrane (OM) (Choi *et al.*, 2011) as previously described. Briefly, WC and OM isolated from

677   *Pto* DC3000 liquid culture (OD$_{600}$ = 3-4). The cells were pelleted via centrifugation (12,000 x

678   g for 10 min). For WC the pellet was resuspended in 1 mL of 20 mM Tris-HCl (pH 8.0), frozen

679   in liquid nitrogen, three times thawing-freezing, and three times sonicated for 10 min at 4 °C.

680   The samples were centrifuged at 6,000 x g for 10 min at 4 °C and supernatants were collected

42

681   and frozen in liquid nitrogen. For OM preparations, the pellet was resuspended in 1 mL 20 mM

682   Tris-HCl (pH 8.0), sucrose (20%), followed by adding 5 uL Lysozyme (15 mg/mL) and 10 µl

683   0.5 M EDTA, incubation for 40 min on ice and adding 20 µL 0.5 M $MgCl_2$. After centrifugation

684   at 9,500 x g for 20 min at 4°C, the pellet was resuspended in 1 mL ice-cold 10 mM Tris-HCl

685   (pH 8.0) followed by sonication three times for 10 min on ice. The samples were then

686   centrifuged at 8,000 x g for 5 min at 4 °C, washed with cold 10 mM Tris-HCl (pH 8.0),

687   resuspend in cold, sterile MilliQ water followed by three times freezing-thawing in liquid

688   nitrogen, incubation for 20 min at 25 °C and adding the sarcosyl to final concentration 0.5%.

689   The samples were then centrifuged at 40,000 x g for 90 min at 4 °C, the pellet was resuspended

690   in ice-cold 10 mM Tris-HCl (pH 8.0) and frozen in liquid nitrogen. Gradient enriched EVs were

691   isolated as above described (Fig. S1C). For proteomics, the samples were denatured by addition

692   of 1 x SDS loading buffer. In-gel trypsin digestion was performed according to standard

693   procedures (Shevchenko *et al.*, 2006). Briefly, 2 µg of EV and OM samples and 20 µg of WC

694   samples were loaded on a NuPAGE 4-12% Bis-Tris Protein gels (Thermofisher Scientific, US),

695   and the gels were run for 3 min only. Subsequently, the still not size-separated single protein

696   band per sample was cut, reduced (50 mM DTT), alkylated (55 mm CAA, chloroacetamid) and

697   digested overnight with trypsin (trypsin-gold, Promega).

698

699   **LC-MS/MS data acquisition**

700   Peptides generated by in-gel trypsin digestion were dried in a vacuum concentrator and

701   dissolved in 0.1% formic acid (FA). LC-MS/MS measurements were performed on a Fusion

702   Lumos Tribrid mass spectrometer (Thermo Fisher Scientific) equipped with an Ultimate 3000

703   RSLCnano system. Peptides were delivered to a trap column (ReproSil-pur C18-AQ, 5 µm, Dr

704   Maisch, 20 mm × 75 µm, self-packed) at a flow rate of 5 µL/min in 100% solvent A (0.1%

705   formic acid in HPLC grade water). After 10 min of loading, peptides were transferred to an

706   analytical column (ReproSil Gold C18-AQ, 3 μm, Dr Maisch, 400 mm × 75 μm, self-packed)

707   and separated using a 50 min gradient from 4% to 32% of solvent B (0.1% formic acid in

708   acetonitrile and 5% (v/v) DMSO) at 300 nL/min flow rate. Both nanoLC solvents contained 5%

709   (v/v) DMSO.

710

711   The Fusion Lumos Tribrid mass spectrometer was operated in data dependent acquisition and

712   positive ionization mode. MS1 spectra (360–1300 m/z) were recorded at a resolution of 60,000

713   using an automatic gain control (AGC) target value of 4e5 and maximum injection time

714   (maxIT) of 50 ms. After peptide fragmentation using higher energy collision induced

715   dissociation (HCD), MS2 spectra of up to 20 precursor peptides were acquired at a resolution

716   of 15.000 with an automatic gain control (AGC) target value of 5e4 and maximum injection

717   time (maxIT) of 22 ms. The precursor isolation window width was set to 1.3 m/z and normalized

718   collision energy to 30%. Dynamic exclusion was enabled with 20 s exclusion time (mass

719   tolerance +/-10 ppm).

720

721   **Computational analysis of proteomes**

722   LFQ values were used in the statistical analysis of proteome data. To select EV-enriched

723   proteins, Welch t-test were used to compare protein intensities between EV and WC samples.

724   The resulted p-values were corrected using the Benjamini-Hochberg method to control the false

725   discovery rate (FDR). The proteins with FDR < 0.05 and with the intensity in EV at least twice

726   higher than in WC were selected as EV-enriched proteins (n = 207). In addition, we selected

727   proteins that were exclusively identified in at least three (out of four) replicates of EV. (n =

728   162). A complete list of EV-enriched proteins is given in Table S1. The functional enrichment

729   analysis of the EV proteins were performed using the DAVID functional annotation tool (Huang

44

730   da *et al.*, 2009a, Huang da *et al.*, 2009b).

731

Database searches

733   Peptide identification and quantification was performed using MaxQuant (version 1.6.3.4) with

734   its built-in search engine Andromeda (Cox *et al.*, 2011, Tyanova *et al.*, 2016). MS2 spectra

735   were searched against a *Pseudomonas syringae pv tomato* protein database (UP000002515,

736   downloaded from Uniprot 04.05.2020) supplemented with common contaminants (built-in

737   option in MaxQuant). For all MaxQuant searches default parameters were employed. Those

738   included carbamidomethylation of cysteine as fixed modification and oxidation of methionine

739   and N-terminal protein acetylation as variable modifications. Trypsin/P was specified as

740   proteolytic enzyme. Precursor tolerance was set to 4.5 ppm, and fragment ion tolerance to 20

741   ppm. Results were adjusted to 1% false discovery rate (FDR) on peptide spectrum match (PSM)

742   and protein level, employing a target-decoy approach using reversed protein sequences. Label-

743   free quantification (LFQ algorithm) was enabled. The minimal peptide length was defined as 7

744   amino acids and the "match-between-run" function was not enabled. Each sample type (EV,

745   OM, WC) was analysed in biological quadruplicates (Table S1).

746

747   We used available localization prediction data at pseudomonas genome database

748   (pseudomonas.com) (Winsor *et al.*, 2016). Predicted protein localizations are presented as

749   stacked bar charts (made in MS Excel) as percentage to total number of the proteins in analyzed

750   sample. We used the available software DAVID bioinformatic resource 6.8

751   (https://david.ncifcrf.gov/) for GO term and KEGG pathway analysis, and the adjusted p-value

752   cut-off was set to 0.05 (Huang da *et al.*, 2009a, Huang da *et al.*, 2009b). We compared the EV

753   enriched proteins from *Pto* DC3000 with EV proteomes from planktonic grown *P. aeruginosa*

754   PAO1 (Choi *et al.*, 2011, Park *et al.*, 2014, Reales-Calderon *et al.*, 2015). We focussed on the

755 proteins that were identified in OMVs from *P. aeruginosa* PAO1 across all three studies and

756 identified their gene orthologs in *Pto* DC3000 using the pseudomonas genome database

757 (pseudomonas.com) (Winsor *et al.*, 2016). This set of proteins was compared to the *Pto* DC3000

758 EV-enriched proteins to predict EV biomarkers. The EV-enriched proteins were also compared

759 with available *in planta Pto* DC3000 transcriptome and proteome data (Nobori *et al.*, 2018)

760 (Nobori *et al.*, 2020).

761

762 **Immunoblot analysis**

763 Standard immunoblot analysis was performed according to Sambrook at al. (1989). 10% SDS-

764 PAGE gels were blotted onto PVDF Immobilon-P membranes (Millipore). *Pto* DC3000 OprF

765 was detected using 1:2,000 diluted rabbit polyclonal antibody against OprF from *Pseudomonas*

766 *aeruginosa* (Cusabio Biotech Co.). As secondary antibody, we used a 1:50,000 dilution of the

767 anti-rabbit IgG-Peroxidase polyclonal antibody (Sigma-Aldrich, A0545). Signal detection was

768 done using SuperSignal West FemtoMaximum Sensitivity Substrate (Pierce, Thermo

769 Scientific), according to manufacturer's instructions, and the images were captured using Vilber

770 Lourmat Peqlab FUSION SL Gel Chemiluminescence Documentation System.

771

772 **Statistical analysis**

773 Student *t*-test, Welsch´s *t*-test, One-way ANOVA followed by Tukey multiple comparisons test

774 and Welsch´s ANOVA with Dunnett´s T3 multiple comparisons post hoc test were performed

775 using GraphPad Prism version 8.3 for Windows, GraphPad Software, San Diego, California

776 USA, www.graphpad.com

777

778 **Data availability**

779 The mass spectrometry proteomics data have been deposited to the ProteomeXchange

780   Consortium via the PRIDE (Perez-Riverol *et al.*, 2019) partner repository with the dataset

781   identifier PXD023971.

782

Author contributions

784   M.J. and S.R. designed research; M.J., C.L., K.R., C.M., L.B., B.S., A.B., A.K. performed

785   research; M.J., C.L., K.R., C.M., A.B., A.K. and S.R. analysed data; E.S., J.S., F.M., J.M.

786   developed protocols; M.J. and S.R. wrote the paper with inputs from all authors.

787

798

799   **Supplemental Information**

800   **Figure S1. A)** The full-size SEM micrograph used in Fig. 1A of *Pto* DC3000 growth in

801   planktonic culture (OD_{600} = 3-4). **B)** Size profile of EVs from *Pto* DC3000 planktonic cultures

802   in fluid samples (OD_{600} = 7.5-11).

803

804   **Figure S2. Isolation of *Pto* DC3000 EVs. A)** Schematic overview of EVs isolation from

805   planktonic cultures for fluid sample (1) and gradient enriched sample (2) analysis. **B)** Growth

806   measurements of planktonic *Pto* DC3000 cultures. Orange indicates EV isolation from early

807   exponential growth stages (OD_{600} = 1-2); green indicates EV isolation from late exponential

808   growth stages (OD_{600} = 3-4). **C)** Schematic overview of EVs isolation from biofilm cultures. **D)**

809   Growth measurements of biofilm *Pto* DC3000 cultures. The green dot represents the growth

810   stage from which the bacteria were used for experiments.

811

812   **Figure S3. Biophysical parameters of particles in apoplastic fluids from *A. thaliana* plants**

813   **infected with *Pto* DC3000. A, D, G)** Particle parameters over days post infection (dpi). **B, E,**

814   **H)** Particle parameters in response to inoculation with different *Pto* DC3000 densities. **C, F, I)**

815   Particle parameters in response to inoculation with different *Pto* DC3000 and co-treatment with

816   flg22. Each dot represents value of independent samples for size and ζ-potential it represents

817   median. 3-12 independent samples were used for each experiment. **J, K)** The profile of ζ-

818   potential for each particle collected from apoplastic fluids of plants treated as indicated and

819   gradient enriched EVs. Control = 0.2 mM EDTA; flg22 = 100 nM; n.t. = not treated; *Pto*

820   DC3000 OD_{600} = 0.0006. Each treatment was 3 days long. The dots represent the mean across

821   the ζ-potential values from independent samples: n = 8 (control); n = 10 (*Pto* DC3000); n = 6

822   (flg22); n = 4 (non-treatment).

823

824 **Figure S4. Pre-treatment with *Pto* DC3000 EVs induces resistance against subsequent *Pto***

825 **DC3000 infection. A)** Three individual biological repeats of *Pto* DC3000 growth (CFU) after

826 infection into leaves of *A. thaliana* without and with EV pre-treatment at 3 dpi (control = 0.02

827 mM EDTA). Each biological repeat consists of 12 independent samples. **B)** *Pto* DC3000 growth

828 (CFU) after infection (3 dpi) into leaves of *A. thaliana* without and with 100 nM flg22 1 day

829 pre-treatment (mock = 10 mM MgCl$_2$) n = 4. Asterisks represent the statistical difference

830 between the treated and control samples (two tailed Student t-test p < 0.01).

831

832 **Figure S5. Characteristics of the proteomic analysis. A)** Barplot shows the number of

833 identified proteins in each replicate. The solid line indicates the cumulative protein IDs and

834 dashed line shows the shared protein IDs. **B)** Boxplot shows a comparable distribution of

835 protein intensities from each replicate.

836

837 **Figure S6. Biophysical parameters of *Pto* DC3000 EVs across isolation methods. A-C)**

838 NTA measurements of particle concentration (A), ζ-potential (B) and size (C) of *Pto* DC3000

839 EVs collected from each step of gradient enrichment. **D-E)** NTA analysis of particle ζ-potential

840 (D) and size (E) of *Pto* DC3000 EVs from fluid samples before (live) and after boiling. Each

841 dot represents an independent sample.

842

843 **Table S1.** Filtered proteomics data with proteins that were identified in at least in three out of

844 four biological repeats in at least one variant (WC, OM and EV). Values used for volcano plot:

845 Highlighted EV-enriched proteins. Subcellar localization of identified proteins. Flagellar

846 proteins identified in EV enriched proteins.

847

848 **Table S2.** GO analysis of EV-enriched proteins

849

850   **Table S3.** Expression of EV-enriched proteins *in planta*

851

852   **Table S4.** *Pseudomonas* EV "core"

853

References

Alves NJ, Turner KB, Medintz IL, Walper SA. 2016. Protecting enzymatic function through directed packaging into bacterial outer membrane vesicles. *Sci Rep* **6**: 24866

Andriankaja A, Boisson-Dernier A, Frances L, Sauviac L, Jauneau A, Barker DG, de Carvalho-Niebel F. 2007. AP2-ERF transcription factors mediate Nod factor dependent Mt ENOD11 activation in root hairs via a novel cis-regulatory motif. *Plant Cell* **19**: 2866-85

Arigita C, Jiskoot W, Westdijk J, van Ingen C, Hennink WE, Crommelin DJ, Kersten GF. 2004. Stability of mono- and trivalent meningococcal outer membrane vesicle vaccines. *Vaccine* **22**: 629-42

Ashburner M, Ball CA, Blake JA, Botstein D, Butler H, Cherry JM, Davis AP, Dolinski K, Dwight SS, Eppig JT, Harris MA, Hill DP, Issel-Tarver L, Kasarskis A, Lewis S, Matese JC, Richardson JE, Ringwald M, Rubin GM, Sherlock G. 2000. Gene ontology: tool for the unification of biology. The Gene Ontology Consortium. *Nat Genet* **25**: 25-9

Bahar O, Mordukhovich G, Luu DD, Schwessinger B, Daudi A, Jehle AK, Felix G, Ronald PC. 2016. Bacterial Outer Membrane Vesicles Induce Plant Immune Responses. *Molecular Plant-Microbe Interactions* **29**: 374-384

Bachurski D, Schuldner M, Nguyen PH, Malz A, Reiners KS, Grenzi PC, Babatz F, Schauss AC, Hansen HP, Hallek M, von Strandmann EP. 2019. Extracellular vesicle measurements with nanoparticle tracking analysis - An accuracy and repeatability comparison between NanoSight NS300 and ZetaView. *Journal of Extracellular Vesicles* **8**

Bauman SJ, Kuehn MJ. 2006. Purification of outer membrane vesicles from Pseudomonas aeruginosa and their activation of an IL-8 response. *Microbes Infect* **8**: 2400-8

Bielska E, Birch PRJ, Buck AH, Abreu-Goodger C, Innes RW, Jin H, Pfaffl MW, Robatzek S, Regev-Rudzki N, Tisserant C, Wang S, Weiberg A. 2019. Highlights of the mini-symposium on extracellular vesicles in inter-organismal communication, held in Munich, Germany, August 2018. *Journal of Extracellular Vesicles* **8**: 1590116

Block A, Alfano JR. 2011. Plant targets for Pseudomonas syringae type III effectors: virulence targets or guarded decoys? *Curr Opin Microbiol* **14**: 39-46

Bredow M, Sementchoukova I, Siegel K, Monaghan J. 2019. Pattern-Triggered Oxidative Burst and Seedling Growth Inhibition Assays in Arabidopsis thaliana. *J Vis Exp*

Buttner D, Bonas U. 2010. Regulation and secretion of Xanthomonas virulence factors. *FEMS Microbiol Rev* **34**: 107-33

Campos ML, de Souza CM, de Oliveira KBS, Dias SC, Franco OL. 2018. The role of antimicrobial peptides in plant immunity. *J Exp Bot* **69**: 4997-5011

Couto D, Zipfel C. 2016. Regulation of pattern recognition receptor signalling in plants. *Nature Reviews Immunology* **16**: 537-52

Couto N, Schooling SR, Dutcher JR, Barber J. 2015. Proteome Profiles of Outer Membrane Vesicles and Extracellular Matrix of Pseudomonas aeruginosa Biofilms. *J Proteome Res* **14**: 4207-22

Cox J, Neuhauser N, Michalski A, Scheltema RA, Olsen JV, Mann M. 2011. Andromeda: a peptide search engine integrated into the MaxQuant environment. *Journal of Proteome Research* **10**: 1794-805

Czechowski T, Stitt M, Altmann T, Udvardi MK, Scheible WR. 2005. Genome-wide identification and testing of superior reference genes for transcript normalization in Arabidopsis. *Plant Physiol* **139**: 5-17

Devos S, Van Oudenhove L, Stremersch S, Van Putte W, De Rycke R, Van Driessche G, Vitse J, Raemdonck K, Devreese B. 2015. The effect of imipenem and diffusible signaling

902 factors on the secretion of outer membrane vesicles and associated Ax21 proteins in
903 Stenotrophomonas maltophilia. *Front Microbiol* **6**: 298

904 **Devos S, Van Putte W, Vitse J, Van Driessche G, Stremersch S, Van Den Broek W,**
905 **Raemdonck K, Braeckmans K, Stahlberg H, Kudryashev M, Savvides SN, Devreese B.**
906 2017. Membrane vesicle secretion and prophage induction in multidrug-resistant
907 Stenotrophomonas maltophilia in response to ciprofloxacin stress. *Environ Microbiol* **19**:
908 3930-3937

909 **Dodds PN, Rathjen JP.** 2010. Plant immunity: towards an integrated view of plant-
910 pathogen interactions. *Nat Rev Genet* **11**: 539-48

911 **Feitosa-Junior OR, Stefanello E, Zaini PA, Nascimento R, Pierry PM, Dandekar AM,**
912 **Lindow SE, da Silva AM.** 2019. Proteomic and Metabolomic Analyses of Xylella fastidiosa
913 OMV-Enriched Fractions Reveal Association with Virulence Factors and Signaling
914 Molecules of the DSF Family. *Phytopathology* **109**: 1344-1353

915 **Figaj D, Ambroziak P, Przepiora T, Skorko-Glonek J.** 2019. The Role of Proteases in the
916 Virulence of Plant Pathogenic Bacteria. *Int J Mol Sci* **20**

917 **Flechsler J, Heimerl T, Pickl C, Rachel R, Stierhof YD, Klingl A.** 2020. 2D and 3D
918 immunogold localization on (epoxy) ultrathin sections with and without osmium
919 tetroxide. *Microsc Res Tech* **83**: 691-705

920 **Frank J, Richter M, de Rossi C, Lehr CM, Fuhrmann K, Fuhrmann G.** 2018. Extracellular
921 vesicles protect glucuronidase model enzymes during freeze-drying. *Sci Rep* **8**: 12377

922 **Hall BM, Breidenstein EBM, de la Fuente-Nunez C, Reffuveille F, Mawla GD, Hancock**
923 **REW, Baker TA.** 2017. Two Isoforms of Clp Peptidase in Pseudomonas aeruginosa
924 Control Distinct Aspects of Cellular Physiology. *Journal of Bacteriology* **199**

925 **Huang da W, Sherman BT, Lempicki RA.** 2009a. Bioinformatics enrichment tools: paths
926 toward the comprehensive functional analysis of large gene lists. *Nucleic Acids Res* **37**: 1-
927 13

928 **Huang da W, Sherman BT, Lempicki RA.** 2009b. Systematic and integrative analysis of
929 large gene lists using DAVID bioinformatics resources. *Nature Protocols* **4**: 44-57

930 **Choi DS, Kim DK, Choi SJ, Lee J, Choi JP, Rho S, Park SH, Kim YK, Hwang D, Gho YS.**
931 2011. Proteomic analysis of outer membrane vesicles derived from Pseudomonas
932 aeruginosa. *Proteomics* **11**: 3424-9

933 **Chowdhury C, Jagannadham MV.** 2013. Virulence factors are released in association
934 with outer membrane vesicles of Pseudomonas syringae pv. tomato T1 during normal
935 growth. *Biochim Biophys Acta* **1834**: 231-9

936 **Ionescu M, Zaini PA, Baccari C, Tran S, da Silva AM, Lindow SE.** 2014. Xylella fastidiosa
937 outer membrane vesicles modulate plant colonization by blocking attachment to surfaces.
938 *Proceedings of the National Academy of Sciences of the United States of America* **111**:
939 E3910-E3918

940 **Kanehisa M, Goto S, Furumichi M, Tanabe M, Hirakawa M.** 2010. KEGG for
941 representation and analysis of molecular networks involving diseases and drugs. *Nucleic*
942 *Acids Res* **38**: D355-60

943 **Kaparakis-Liaskos M, Ferrero RL.** 2015. Immune modulation by bacterial outer
944 membrane vesicles. *Nature Reviews Immunology* **15**: 375-387

945 **Klimentova J, Stulik J.** 2015. Methods of isolation and purification of outer membrane
946 vesicles from gram-negative bacteria. *Microbiol Res* **170**: 1-9

947 **Knoke LR, Abad Herrera S, Gotz K, Justesen BH, Gunther Pomorski T, Fritz C,**
948 **Schakermann S, Bandow JE, Aktas M.** 2020. Agrobacterium tumefaciens Small
949 Lipoprotein Atu8019 Is Involved in Selective Outer Membrane Vesicle (OMV) Docking to
950 Bacterial Cells. *Front Microbiol* **11**: 1228

951 **Krckova Z, Kocourkova D, Danek M, Brouzdova J, Pejchar P, Janda M, Pokotylo I, Ott**
952 **PG, Valentova O, Martinec J.** 2018. The Arabidopsis thaliana non-specific phospholipase
953 C2 is involved in the response to Pseudomonas syringae attack. *Annals of Botany* **121**:
954 297-310

955 **Kunze G, Zipfel C, Robatzek S, Niehaus K, Boller T, Felix G.** 2004. The N terminus of
956 bacterial elongation factor Tu elicits innate immunity in Arabidopsis plants. *Plant Cell* **16**:
957 3496-3507

958 **Kvitko BH, Park DH, Velasquez AC, Wei CF, Russell AB, Martin GB, Schneider DJ,**
959 **Collmer A.** 2009. Deletions in the repertoire of Pseudomonas syringae pv. tomato DC3000
960 type III secretion effector genes reveal functional overlap among effectors. *Plos Pathogens*
961 **5**: e1000388

962 **Lappann M, Otto A, Becher D, Vogel U.** 2013. Comparative proteome analysis of
963 spontaneous outer membrane vesicles and purified outer membranes of Neisseria
964 meningitidis. *Journal of Bacteriology* **195**: 4425-35

965 **Lovelace AH, Smith A, Kvitko BH.** 2018. Pattern-Triggered Immunity Alters the
966 Transcriptional Regulation of Virulence-Associated Genes and Induces the Sulfur
967 Starvation Response in Pseudomonas syringae pv. tomato DC3000. *Mol Plant Microbe*
968 *Interact* **31**: 750-765

969 **Macdonald IA, Kuehn MJ.** 2013. Stress-induced outer membrane vesicle production by
970 Pseudomonas aeruginosa. *Journal of Bacteriology* **195**: 2971-81

971 **Manabe T, Kato M, Ueno T, Kawasaki K.** 2013. Flagella proteins contribute to the
972 production of outer membrane vesicles from Escherichia coli W3110. *Biochem Biophys*
973 *Res Commun* **441**: 151-6

974 **Mansfield J, Genin S, Magori S, Citovsky V, Sriariyanum M, Ronald P, Dow M, Verdier**
975 **V, Beer SV, Machado MA, Toth I, Salmond G, Foster GD.** 2012. Top 10 plant pathogenic
976 bacteria in molecular plant pathology. *Molecular Plant Pathology* **13**: 614-629

977 **McBroom AJ, Johnson AP, Vemulapalli S, Kuehn MJ.** 2006. Outer membrane vesicle
978 production by Escherichia coli is independent of membrane instability. *Journal of*
979 *Bacteriology* **188**: 5385-5392

980 **McBroom AJ, Kuehn MJ.** 2007. Release of outer membrane vesicles by Gram-negative
981 bacteria is a novel envelope stress response. *Mol Microbiol* **63**: 545-58

982 **McCaig WD, Koller A, Thanassi DG.** 2013. Production of outer membrane vesicles and
983 outer membrane tubes by Francisella novicida. *Journal of Bacteriology* **195**: 1120-32

984 **McMillan HM, Zebell SG, Ristaino JB, Dong X, Kuehn MJ.** 2020. Protective Plant Immune
985 Responses are Elicited by Bacterial Outer Membrane Vesicles. *BioRxiv*

986 **Melotto M, Underwood W, Koczan J, Nomura K, He SY.** 2006. Plant stomata function in
987 innate immunity against bacterial invasion. *Cell* **126**: 969-80

988 **Mersmann S, Bourdais G, Rietz S, Robatzek S.** 2010. Ethylene signaling regulates
989 accumulation of the FLS2 receptor and is required for the oxidative burst contributing to
990 plant immunity. *Plant Physiology* **154**: 391-400

991 **Metruccio MM, Evans DJ, Gabriel MM, Kadurugamuwa JL, Fleiszig SM.** 2016.
992 Pseudomonas aeruginosa Outer Membrane Vesicles Triggered by Human Mucosal Fluid
993 and Lysozyme Can Prime Host Tissue Surfaces for Bacterial Adhesion. *Front Microbiol* **7**:
994 871

995 **Nascimento R, Gouran H, Chakraborty S, Gillespie HW, Almeida-Souza HO, Tu A, Rao**
996 **BJ, Feldstein PA, Bruening G, Goulart LR, Dandekar AM.** 2016. The Type II Secreted
997 Lipase/Esterase LesA is a Key Virulence Factor Required for Xylella fastidiosa
998 Pathogenesis in Grapevines. *Scientific Reports* **6**

999 **Nobori T, Velasquez AC, Wu JN, Kvitko BH, Kremer JM, Wang Y, He SY, Tsuda K.** 2018.
1000 Transcriptome landscape of a bacterial pathogen under plant immunity. *Proceedings of*
1001 *the National Academy of Sciences of the United States of America* **115**: E3055-E3064
1002 **Nobori T, Wang Y, Wu J, Stolze SC, Tsuda Y, Finkemeier I, Nakagami H, Tsuda K.** 2020.
1003 Multidimensional gene regulatory landscape of a bacterial pathogen in plants. *Nat Plants*
1004 **Nobori T, Yiming W, Jingni W, Christina SS, Yayoi T, Iris F, Hirofumi N, Kenichi T.**
1005 2019. In planta bacterial multi-omics analysis illuminates regulatory principles
1006 underlying plant-pathogen interactions. *BioRxiv*
1007 **Nomura K, Debroy S, Lee YH, Pumplin N, Jones J, He SY.** 2006. A bacterial virulence
1008 protein suppresses host innate immunity to cause plant disease. *Science* **313**: 220-3
1009 **Park AJ, Murphy K, Krieger JR, Brewer D, Taylor P, Habash M, Khursigara CM.** 2014.
1010 A temporal examination of the planktonic and biofilm proteome of whole cell
1011 Pseudomonas aeruginosa PAO1 using quantitative mass spectrometry. *Mol Cell*
1012 *Proteomics* **13**: 1095-105
1013 **Perez-Cruz C, Delgado L, Lopez-Iglesias C, Mercade E.** 2015. Outer-inner membrane
1014 vesicles naturally secreted by gram-negative pathogenic bacteria. *Plos One* **10**: e0116896
1015 **Perez-Riverol Y, Csordas A, Bai J, Bernal-Llinares M, Hewapathirana S, Kundu DJ,**
1016 **Inuganti A, Griss J, Mayer G, Eisenacher M, Perez E, Uszkoreit J, Pfeuffer J,**
1017 **Sachsenberg T, Yilmaz S, Tiwary S, Cox J, Audain E, Walzer M, Jarnuczak AF** *et al.*
1018 2019. The PRIDE database and related tools and resources in 2019: improving support
1019 for quantification data. *Nucleic Acids Res* **47**: D442-D450
1020 **Prados-Rosales R, Weinrick BC, Pique DG, Jacobs WR, Jr., Casadevall A, Rodriguez**
1021 **GM.** 2014. Role for Mycobacterium tuberculosis membrane vesicles in iron acquisition.
1022 *Journal of Bacteriology* **196**: 1250-6
1023 **Raposo G, Stoorvogel W.** 2013. Extracellular vesicles: exosomes, microvesicles, and
1024 friends. *J Cell Biol* **200**: 373-83
1025 **Reales-Calderon JA, Corona F, Monteoliva L, Gil C, Martinez JL.** 2015. Quantitative
1026 proteomics unravels that the post-transcriptional regulator Crc modulates the generation
1027 of vesicles and secreted virulence determinants of Pseudomonas aeruginosa. *Data Brief*
1028 **4**: 450-3
1029 **Roier S, Zingl FG, Cakar F, Durakovic S, Kohl P, Eichmann TO, Klug L, Gadermaier B,**
1030 **Weinzerl K, Prassl R, Lass A, Daum G, Reidl J, Feldman MF, Schild S.** 2016. A novel
1031 mechanism for the biogenesis of outer membrane vesicles in Gram-negative bacteria.
1032 *Nature Communications* **7**: 10515
1033 **Rossbach S, Wilson TL, Kukuk ML, Carty HA.** 2000. Elevated zinc induces siderophore
1034 biosynthesis genes and a zntA-like gene in Pseudomonas fluorescens. *FEMS Microbiol Lett*
1035 **191**: 61-70
1036 **Roszkowiak J, Jajor P, Gula G, Gubernator J, Zak A, Drulis-Kawa Z, Augustyniak D.**
1037 2019. Interspecies Outer Membrane Vesicles (OMVs) Modulate the Sensitivity of
1038 Pathogenic Bacteria and Pathogenic Yeasts to Cationic Peptides and Serum Complement.
1039 *Int J Mol Sci* **20**
1040 **Rutter BD, Innes RW.** 2017. Extracellular Vesicles Isolated from the Leaf Apoplast Carry
1041 Stress-Response Proteins. *Plant Physiology* **173**: 728-741
1042 **Rybak K, Robatzek S.** 2019. Functions of Extracellular Vesicles in Immunity and
1043 Virulence. *Plant Physiology* **179**: 1236-1247
1044 **Sampath V, McCaig WD, Thanassi DG.** 2018. Amino acid deprivation and central carbon
1045 metabolism regulate the production of outer membrane vesicles and tubes by Francisella.
1046 *Mol Microbiol* **107**: 523-541

1047 **Shevchenko A, Tomas H, Havlis J, Olsen JV, Mann M.** 2006. In-gel digestion for mass
1048 spectrometric characterization of proteins and proteomes. *Nat Protoc* **1**: 2856-60
1049 **Schechter LM, Vencato M, Jordan KL, Schneider SE, Schneider DJ, Collmer A.** 2006.
1050 Multiple approaches to a complete inventory of Pseudomonas syringae pv. tomato
1051 DC3000 type III secretion system effector proteins. *Mol Plant Microbe Interact* **19**: 1180-
1052 92
1053 **Schindelin J, Arganda-Carreras I, Frise E, Kaynig V, Longair M, Pietzsch T, Preibisch
1054 S, Rueden C, Saalfeld S, Schmid B, Tinevez JY, White DJ, Hartenstein V, Eliceiri K,
1055 Tomancak P, Cardona A.** 2012. Fiji: an open-source platform for biological-image
1056 analysis. *Nat Methods* **9**: 676-82
1057 **Schwechheimer C, Kuehn MJ.** 2015. Outer-membrane vesicles from Gram-negative
1058 bacteria: biogenesis and functions. *Nature Reviews Microbiology* **13**: 605-619
1059 **Sidhu VK, Vorholter FJ, Niehaus K, Watt SA.** 2008. Analysis of outer membrane vesicle
1060 associated proteins isolated from the plant pathogenic bacterium Xanthomonas
1061 campestris pv. campestris. *Bmc Microbiology* **8**
1062 **Sole M, Scheibner F, Hoffmeister AK, Hartmann N, Hause G, Rother A, Jordan M,
1063 Lautier M, Arlat M, Buttner D.** 2015. Xanthomonas campestris pv. vesicatoria Secretes
1064 Proteases and Xylanases via the Xps Type II Secretion System and Outer Membrane
1065 Vesicles. *Journal of Bacteriology* **197**: 2879-2893
1066 **The Gene Ontology C.** 2019. The Gene Ontology Resource: 20 years and still GOing
1067 strong. *Nucleic Acids Res* **47**: D330-D338
1068 **Toyofuku M, Nomura N, Eberl L.** 2019. Types and origins of bacterial membrane
1069 vesicles. *Nature Reviews Microbiology* **17**: 13-24
1070 **Turnbull L, Toyofuku M, Hynen AL, Kurosawa M, Pessi G, Petty NK, Osvath SR,
1071 Carcamo-Oyarce G, Gloag ES, Shimoni R, Omasits U, Ito S, Yap X, Monahan LG,
1072 Cavaliere R, Ahrens CH, Charles IG, Nomura N, Eberl L, Whitchurch CB.** 2016.
1073 Explosive cell lysis as a mechanism for the biogenesis of bacterial membrane vesicles and
1074 biofilms. *Nature Communications* **7**: 11220
1075 **Tyanova S, Temu T, Cox J.** 2016. The MaxQuant computational platform for mass
1076 spectrometry-based shotgun proteomics. *Nat Protoc* **11**: 2301-2319
1077 **Vinatzer BA, Teitzel GM, Lee MW, Jelenska J, Hotton S, Fairfax K, Jenrette J,
1078 Greenberg JT.** 2006. The type III effector repertoire of Pseudomonas syringae pv.
1079 syringae B728a and its role in survival and disease on host and non-host plants. *Mol
1080 Microbiol* **62**: 26-44
1081 **Wan WL, Frohlich K, Pruitt RN, Nurnberger T, Zhang L.** 2019. Plant cell surface
1082 immune receptor complex signaling. *Current Opinion in Plant Biology* **50**: 18-28
1083 **Wang Y, Garrido-Oter R, Wu J, Winkelmuller TM, Agler M, Colby T, Nobori T, Kemen
1084 E, Tsuda K.** 2019. Site-specific cleavage of bacterial MucD by secreted proteases mediates
1085 antibacterial resistance in Arabidopsis. *Nature Communications* **10**: 2853
1086 **Wei HL, Zhang W, Collmer A.** 2018. Modular Study of the Type III Effector Repertoire in
1087 Pseudomonas syringae pv. tomato DC3000 Reveals a Matrix of Effector Interplay in
1088 Pathogenesis. *Cell Rep* **23**: 1630-1638
1089 **Wilson M, Campbell HL, Ji P, Jones JB, Cuppels DA.** 2002. Biological control of bacterial
1090 speck of tomato under field conditions at several locations in north america.
1091 *Phytopathology* **92**: 1284-92
1092 **Winsor GL, Griffiths EJ, Lo R, Dhillon BK, Shay JA, Brinkman FS.** 2016. Enhanced
1093 annotations and features for comparing thousands of Pseudomonas genomes in the
1094 Pseudomonas genome database. *Nucleic Acids Res* **44**: D646-53

1095   **Xin XF, He SY.** 2013. Pseudomonas syringae pv. tomato DC3000: a model pathogen for
1096   probing disease susceptibility and hormone signaling in plants. *Annu Rev Phytopathol* **51**:
1097   473-98
1098   **Xin XF, Kvitko B, He SY.** 2018. Pseudomonas syringae: what it takes to be a pathogen.
1099   *Nature Reviews Microbiology* **16**: 316-328
1100   **Zingl FG, Kohl P, Cakar F, Leitner DR, Mitterer F, Bonnington KE, Rechberger GN,**
1101   **Kuehn MJ, Guan Z, Reidl J, Schild S.** 2020. Outer Membrane Vesiculation Facilitates
1102   Surface Exchange and In Vivo Adaptation of Vibrio cholerae. *Cell Host & Microbe* **27**: 225-
1103   237 e8
1104   **Zipfel C, Kunze G, Chinchilla D, Caniard A, Jones JD, Boller T, Felix G.** 2006. Perception
1105   of the bacterial PAMP EF-Tu by the receptor EFR restricts Agrobacterium-mediated
1106   transformation. *Cell* **125**: 749-60
1107   **Zipfel C, Robatzek S, Navarro L, Oakeley EJ, Jones JD, Felix G, Boller T.** 2004. Bacterial
1108   disease resistance in Arabidopsis through flagellin perception. *Nature* **428**: 764-7
1109